Satellite-derived SO_2 flux time-series and magmatic processes during the 2015 Calbuco eruptions

Federica Pardini[1], Mike Burton[1], Fabio Arzilli[1], Giuseppe La Spina[1], Margherita Polacci[1]

[1]School of Earth and Environmental Science, University of Manchester, Manchester, M13 9PL, UK

Correspondence to: Federica Pardini (federica.pardini@manchester.ac.uk)

Abstract. Quantifying time-series of ~~sulphur~~ sulfur dioxide (SO_2) emissions during explosive eruptions provides insight into volcanic processes, assists in volcanic hazard mitigation, and permits quantification of the climatic impact of major eruptions. While volcanic SO_2 is routinely detected from space during eruptions, the retrieval of plume injection height and SO_2 flux time-series remains challenging. Here we present a new numerical method based on forward- and backward-trajectory analyses which enable such time-series to be robustly determined. ~~The method is applied to satellite images of volcanic eruption clouds through the integration of the HYSPLIT software with custom designed Python routines in a fully automated manner. Plume injection height and SO_2 flux time-series are computed with a period of ~10 minutes with low computational cost.~~

Using this technique, we investigated the SO_2 emissions from two sub-Plinian eruptions of Calbuco, Chile, produced in April 2015. We found a mean injection height above the vent of ~15 km for the two eruptions, with overshooting tops reaching ~20 km. We calculated a total of 300±46 ~~kt~~ kt of SO_2 released almost equally during both events, with 160±30 kt produced by the first event and 140±35 kt by the second one. ~~The retrieved SO_2 flux time-series show an intense gas release during the first eruption (average flux of 2560 kt day^{-1}), while a lower SO_2 flux profile was seen for the second (average flux 560 kt day^{-1}), suggesting that the first eruption was richer in SO_2. This result is exemplified by plotting SO_2 flux against retrieved plume height above the vent, revealing distinct trends for the two events.~~ From our satellite derived results, we inferred the presence of pre-eruptive exsolved SO_2 for both the eruptions, with the first event richer in pre-eruptive SO_2 than the second one. ~~We propose that a pre-erupted exsolved volatile phase was present prior to the first event, which could have led to the necessary overpressure to trigger the eruption. The second eruption, instead, was mainly driven by syneruptive degassing.~~ This hypothesis is supported by melt inclusions measurements of sulfur concentrations in plagioclase phenocrysts and groundmass glass of tephra samples through electron microprobe analysis. We propose that the overpressure caused by the pre-exsolved volatile phase (not only SO_2, but also probably H_2O and CO_2) may have triggered the two sub-Plinian eruptions.

This work demonstrates that detailed interpretations of sub-surface magmatic processes during eruptions are possible using satellite SO_2 data. ~~Quantitative comparisons of high temporal resolution plume height and SO_2 flux time-series offer a powerful tool to examine processes triggering and controlling eruptions.~~ These novel tools open a new frontier in space-based volcanological research, and will be of great value when applied to remote, poorly monitored volcanoes, and to major eruptions

that can have regional and global climate implications through, for example, influencing ozone depletion in the stratosphere and light scattering from stratospheric aerosols.

1 Introduction

Understanding the manner and the abundance of sulfur degassing from active volcanoes during explosive eruptions is one key to unravelling eruptive dynamics (Oppenheimer et al., 2011, Wallace and Edmonds, 2011). At a volcanic vent, sulfur gases contribute 2-35 vol% of total gas emissions, with SO_2 and H_2S the dominant sulfur-bearing components, ranging between 1-25 vol% and 1-10 vol% respectively (Textor et al., 2004). Satellite-based instruments operating in the ultraviolet and infrared have detected and quantified volcanic sulfur gases in the atmosphere since 1978 (Carn et al., 2016). Nowadays, this is routinely done for SO_2 (Brenot et al., 2014), while few H_2S satellite retrievals have been performed so far (Clarisse et al., 2011). Satellite-based monitoring of volcanic SO_2 emissions is of value for poorly monitored volcanoes, which make up almost 95% of all volcanoes, but are also useful when well-monitored volcanoes erupt explosively, as local detection system can be saturated or blinded by ash.

Satellite images of volcanic SO_2 plumes contain a lot of information ~~which~~ that can be extracted with the appropriate data analysis approach (McCormick et al., 2014; Hayer et al., 2016). The most immediate information is typically vertical column amounts of SO_2 which can be readily used to determine a total SO_2 mass loading, and this is the most frequently used type of data provided in the literature. Valuable time-series information on SO_2 injection height and SO_2 flux time-series are also theoretically available, and these allow subtle observations and deductions on the volcanic processes driving eruptions, including magma degassing (Carn et al., 2008; Carn and Prata 2010; Campion 2014) and the role of pre-eruptive gas accumulation (Westrich et ~~al.~~Gerlach, 1992). While a lot of work has been done on SO_2 satellite retrievals, a comprehensive, general methodology able to fully characterize both SO_2 flux and plume height time-series has not been successfully created to date. This is mainly due to the difficulty in retrieving SO_2 vertical profiles for individual SO_2 column amount pixels in an image. All satellite-based SO_2 column amount calculations are dependent on both the measured SO_2 optical depth and the plume height, and so quantification of SO_2 amounts requires an accurate determination of plume height pixel by pixel in an image. Plume heights have been retrieved using infrared and ultraviolet spectra (Yang et al., 2010; Nowlan et al., 2011; Rix et al., 2012; Carboni et al., 2012; Carboni et al., 2016; Grainger et al., 2016) and from numerical models applied to satellite images (Hughes et al., 2012; Clarisse et al., 2014; Moxnes et al., 2014; Heng et al., 2016; Pardini et al., 2017).

SO_2 flux time-series can be calculated from satellite imagery using a variety of methods (a review is presented in Theys et al., (2011)). Four methodologies have been applied: the box method (Lopez et al., 2013), the traverse method (Merucci et al., 2011), the delta method (Krueger et al., 1996) and inverse modelling (Eckhardt et al., 2008, Boichu et al., 2013). Depending on the input parameters (plume age at the measurement time, satellite sensor spatial resolution, number of satellite acquisitions in a day, etc…) and expected outcomes (flux time-series, plume height time-series), each method has strengths and weaknesses. The b~~B~~ox method is suitable for a first flux evaluation, but it needs constant wind speed and direction together with an *a-*

priori estimation of plume height. The traverse method has been used to compare fluxes retrieved from satellite-based instruments with those from ground based measurements. This technique allows an almost real time estimate of SO_2 fluxes, ~~despite~~ but it needs constant wind direction and plume height as input data. The ~~box method~~delta method is independent from wind speed and it produces an estimate of the SO_2 lifetime, however multiple satellite overpasses are needed. Finally, the inverse modelling allows us to compute fluxes at high temporal resolution even for plume presenting a complex vertical profile. The main drawback of this technique is the computational time.

In this work, we investigate SO_2 emissions during explosive eruptions with the aim of exhaustively examining the information which can be obtained from satellite imagery. We do this through application of a back-trajectory model to determine both the plume height for each SO_2 pixel in the satellite image, and the time at which the SO_2 in each pixel~~'s SO_2~~ was injected into the atmosphere. We adapted the Hybrid Single-Particle Lagrangian Integrated Trajectory model (HYSPLIT) (Stein at al., 2015) by ~~integration~~ integrating it with custom-built Python routines in order to create a semi-automated numerical procedure from which injection height and flux time-series are computed at high temporal resolution.

The algorithm we have implemented allow us to study both explosive and effusive eruptions, and, for each case study, specific input parameters (such as volcanic location, type of eruption, eruption time) can be set by the user. Our technique requires satellite and wind field datasets, which can derive from a variety of sources. Indeed, many satellite sensors can ~~detect~~ measure volcanic SO_2 atmospheric abundance (Carn et al., 2016), and, theoretically, each satellite dataset can be used as input for ~~the~~ our model. The same can be done for the wind field data, ~~which, however, has to~~ if it is ~~be written~~ in ~~a format that~~ HYSPLIT-readable format ~~can read~~. Our algorithm is fast (<12 h on one PC, <3 h on a cluster) and it does not require constant wind speed or multiple satellite overpasses. The main advantage is the possibility to retrieve both SO_2 plume height and flux at high temporal and spatial resolution. ~~However, r~~Results rely on the accuracy of wind field datasets, ~~which could potentially affect the retrieved SO_2 abundances.~~ so wind field errors can propagate into retrieved SO_2 errors, as is the case for most flux calculations. Our algorithm can be applied to a single image, using back-trajectory modelling, or image pairs, examining both forward and backward trajectories and thereby reducing wind field errors.

We applied our numerical method to GOME-2 satellite images of SO_2 plumes emitted by the two recent sub-Plinian eruptions occurred at Calbuco volcano, Chile, in April 2015. The eruptions have been classified as VEI 4 (Romero et al., 2016) and led to ozone depletion in Antarctica (Solomon et al., 2016, Ivy et al., 2017).

Our retrieved SO_2 injection height and flux time-series, together with estimates of masses of erupted material, allow us to infer the presence of excess SO_2 at depth before the eruptions. ~~Furthermore, i~~In order to validate and quantify the amount of excess SO_2, we performed microprobe analysis of melt inclusions in plagioclase phenocrysts and ground mass of erupted products. This allows us to compare our numerical results with the SO_2 loading derived from the ~~"P~~petrological ~~Method"~~ method (Devine et al., 1984; Sigmarsson et al., 2013), which uses~~s~~ information on the mass loading of each eruption and the volatile loss inferred from the difference in sulfur concentration between melt inclusions and groundmass.

2 Case study: the 22-23 April 2015 Calbuco eruptions

On the evening of 22 April 2015, Calbuco volcano started a new cycle of eruptive activity after 54 years of quiescence. Calbuco [~~(~~41.33° S, 72.61° W] is an active stratovolcano located in the southern region of the Southern Volcanic Zone of the Andes, Chile. It has been volcanically active since the Late Pleistocene to the present, with the formation of 4 principle deposits. The last deposit has a "dome-cone" structure resulting from a series of recent major eruptions which occurred in 1912, 1961, 1971 and 1983-94 (Lopez-Escobar et al., 1992). The new eruptive cycle started on 22 April 2015 and lasted 9 days, until 30 April 2015. An initial sub-Plinian eruption took place on the evening of 22 April (hereafter Eruption 1), and a second eruption occurred a few hours later in the morning of 23 April (hereafter Eruption 2).

Eruption 1 started suddenly at 20:54 UT. A volcanic column more than 15 km height rose from the main crater and tephra was dispersed in an East-Northeast direction. The overall duration of the event was 1.5 h. After Eruption 1 stopped, moderate seismic events in the form of volcanic tremor were recorded from 00:55 UT. At 04:00 UT, a new eruptive event (Eruption 2) occurred. The intensity of the ~~The~~ second eruption appeared to ~~be more violent than the first one and lasted several hours~~be higher than the first one and with a ~50 % greater mass eruption rate (Van Eaton et al., 2016). The eruptive column reached more than 15 km in altitude and tephra was dispersed in a North, Northeast and East direction. At 10:30 UT the eruption was declared over (SERNAGEOMIN, 2015a, 2015b, 2015c).

The eruptions are classified as VEI 4 (Romero et al., 2016) and they produced columns reaching the stratosphere (Begue et al., 2017). The stratospheric injection by the volcanic cloud together with the latitude of Calbuco, produced an impact on ozone recovery in Antarctica causing an increase in hole size of 4.4 million km^2 (Solomon et al., 2106; Ivy et al., 2017). Moreover, extensive damage was caused to the Chilean economy, with agricultural and industrial resources close to Calbuco damaged by ash fall, and air traffic over Chile and Argentina disrupted for some hours (Romero et al., 2016).

Considering both the tephra fall and PDC deposits, the deposit volume estimated by Castruccio et al., (2016) is 0.38 km^3 assuming a deposit density of 1000 kg m^{-3} (0.15 km^3 dense rock equivalent DRE ~~assuming a deposit density 1000 kg m^{-3}~~), while Romero et al., (2016)~~)~~ report a tephra fall deposit volume of 0.28 km^3 considering a deposit density of 997.3 kg m^{-3} (0.11-0.13 km^3 DRE ~~using a density of 2450 km m^{-3} for the 80% low density deposit and 2500 kg m^{-3} for the remain 20%~~). These values are both within the 0.56±0.28 km^3 volume calculated by Van Eaton et al., (2016), which presents a DRE of 0.18±0.09 km^3 assuming a magma density of 2500 kg m^{-3}.

3 Methods

3.1 Backward and Forward Trajectory Model

The numerical procedure used here is a development of that presented by Pardini et al., (2017). This new approach uses a two-step procedure based on a combination of forward and backward trajectories applied to a pair of images in order to decrease the uncertainties on the results arising from wind field errors. We also modified the ~~post processing phase~~ algorithm compared with Pardini et al., (2017) ~~,~~by changing the selection criteria for acceptable trajectories by including the independently-

observed eruption time and umbrella growth. ~~and adding~~ We also added an SO_2 flux calculation. Due to the general implementation of the procedure, it can be easily applied to different volcanic systems to investigate SO_2 emissions during eruptive episodes or produced by quiescent degassing. In order to run the algorithm, we ideally require two satellite images capturing the same volcanic plume at different times~~, are required, as well as~~ wind fields for each image capture time, and independent observations of the eruption onset and duration. For each pixel of the computational domain in which SO_2 is detected, the method proposed here calculates three quantities. The first quantity, h, is the height at which the SO_2 is located at satellite measurement time instant (hereafter plume height). The second ~~one~~quantity, h_{vent}, is the height above volcanic vent at which SO_2 reaches the neutral buoyancy height and the prevailing atmospheric wind starts to disperse the gas into the atmosphere (hereafter injection height). The last ~~one~~quantity, t_{vent}, is the time when the SO_2 reaches the injection height (hereafter injection time). Knowing these three quantities and SO_2 column amount from satellite images, we ~~are able to~~ calculate the SO_2 mass loading of the plume and SO_2 flux time-series at ~~a~~ the volcanic vent.

Plume parameters are computed by calculating trajectories run forwards and backwards in time. The trajectory calculation is performed by using HYSPLIT (Stein et al., 2015) with custom-designed routines written in the Python Programming Language.

The two-step procedure is done by using two satellite images collected at different times of ~~a~~ the same volcanic SO_2 plume. The first image captures the SO_2 plume at day ~~ik~~, while the second image at day ~~ik~~ $+ 1$.

In Figure 1 we illustrate a schematic description of the technique used here. With the green pixels we indicate the region of the computational domain of the day ~~ik~~ satellite image where SO_2 is detected, whilst with the yellow pixels we show the SO_2 plume captured at day ~~ik~~ $+ 1$. For each pixel j where SO_2 is detected and for each potential plume height~~s~~ $h_j(i)$ in a given range, we calculate forward trajectories $traj_j^f(i)$ up to the time of acquisition of the day ~~ik~~ $+ 1$ image. Among these trajectories, only those consistent with the advected/dispersed plume at day ~~ik~~ $+ 1$ are considered (for example, in Figure 1 only $traj_j^f(1)$ and $traj_j^f(3)$ are acceptable). Then, starting only from $h_j(i)$ of each acceptable forward trajectory, we calculate backward trajectories $traj_j^b(i)$. We then select as acceptable trajectories only those approaching the volcanic vent location within a certain threshold distance and within the time interval of the eruption (for example, in Figure 1 only $traj_j^b(1)$ is acceptable). We adopt this two-step trajectory analysis to decrease the uncertainties on plume parameters due to wind field errors.

The definition of an acceptable threshold distance from the ventfor calculated back-trajectories relies on physical constraints. ~~Indeed~~Here, we calculate this~~e~~ threshold distance ~~of approach is set~~ according to the growth of the umbrella cloud radius (r) during the eruption. Thus, we consider acceptable a backward trajectory ~~which~~ whose minimal distance from the volcanic vent is less than r. Following Sparks et al., (1997), the radius of an umbrella cloud growing with time at the neutral buoyancy height can be expressed as:

$$r(t) = \left(\frac{3\lambda}{2\pi} N \cdot MER\right)^{\frac{1}{3}} t^{\frac{2}{3}}, \quad (1)$$

where λ is an empirical constant, N is the buoyancy frequency of the atmosphere and MER is the mass flow rate at buoyancy height. Following Sparks et al., (1997), we set λ equal to 0.8 and N equal to 0.17 for stratospheric strong plumes.

Using the two step procedure previously described, ~~F~~for each pixel j of the computational domain, and for each acceptable backward trajectory $traj_j^b(i)$ starting from the pixel j, we extract the three plume parameters, $h_j(i)$, $h_{j_{vent}}(i)$ and $t_{j_{vent}}(i)$. The height $h_j(i)$ is the altitude of the starting point of the backward trajectory $traj_j^b(i)$ of the pixel j. Instead, $h_{j_{vent}}(i)$ and $t_{j_{vent}}(i)$ are respectively the height and the time at which each acceptable backward trajectory $traj_j^b(i)$ approaches the vent. From the plume parameters calculated by our numerical method, we compute, for each pixel j, the mean values ($\bar{h}_j$, $\bar{h}_{j_{vent}}$ and $\bar{t}_{j_{vent}}$) and standard deviations (σ_{j_h}, $\sigma_{j_{h_{vent}}}$ and $\sigma_{j_{t_{vent}}}$) as:

$$\bar{h} = \sum_{i=1}^{N} \frac{h_j(i)}{N}, \quad (2)$$

$$\bar{h}_{j_{vent}} = \sum_{i=1}^{N} \frac{h_{j_{vent}}(i)}{N}, \quad (3)$$

$$\bar{t}_{j_{vent}} = \sum_{i=1}^{N} \frac{t_{j_{vent}}(i)}{N}, \quad (4)$$

$$\sigma_{j_h} = \sum_{i=1}^{N} \frac{(h_j(i) - \bar{h})^2}{N}, \quad (5)$$

$$\sigma_{j_{h_{vent}}} = \sum_{i=1}^{N} \frac{(h_{j_{vent}}(i) - \bar{h}_{j_{vent}})^2}{N}, \quad (6)$$

$$\sigma_{j_{t_{vent}}} = \sum_{i=1}^{N} \frac{(t_{j_{vent}}(i) - \bar{t}_{j_{vent}})^2}{N}, \quad (7)$$

where N is the number of backward trajectories $traj_j^b(i)$ that approach the vent, $h_j(i)$ is the altitude from which trajectories are initialized, while $t_{j_{vent}}(i)$ and $h_{j_{vent}}(i)$ are the time instant and the altitude of approach at vent position.

Using these data, we ~~can~~ compute the SO_2 ~~mass~~ loading in the volcanic plume and the mass of the erupted tephra ~~fall deposit~~. Finally, by associating pixels injection times ($t_{j_{vent}}$) with their SO_2 mass loading, which is calculated from satellite SO_2 column amount, we calculate SO_2 flux time-series.

3.2 Petrological Method to Estimate Sulfur in Magma

To quantify the atmospheric sulfur yield from the Calbuco eruptions, we adopt a well-established petrological method (Devine et al., 1984; Sigmarsson et al., 2013). The method consists of measuring the sulfur concentration in glassy melt inclusions, which represent the undegassed melt, and in matrix glasses, which instead represent the degassed melt. The mass of sulfur released is then calculated by the difference of the two concentrations multiplied by the mass of erupted material. A correction taking into account the mass fraction of syn- or post-eruptive crystals can also be considered. In order to compare our satellite estimates of SO_2 mass loadings with elemental sulfur concentrations, it is useful to convert petrological estimates of sulfur mass loadings into SO_2 mass loadings. This is readily achieved by multiplying by two, following the molecular weight of SO_2 (64 g mol^{-1}) and atomic weight of sulfur (32 g mol^{-1}). Thus, according to the petrological method, the SO_2 loading released into the atmosphere during an individual eruption ($m(SO_2)_{PETR}$) can be expressed as:

$$m(SO_2)_{PETR} = M \cdot (S_{MI} - S_{gm}) \cdot \frac{MW(SO_2)}{MW(S)} \cdot (1 - CF), \quad (8)$$

where M is the mass of erupted material, S_{MI} and S_{gm} are the sulfur concentrations measured in melt inclusions and glassy matrix, $MW(SO_2)$ and $MW(S)$ are the molecular weights of SO_2 and S and CF is a coefficient accounting for the volume of syn- or post-eruptive crystals in the melt. This method has been applied often in conjunction with satellite estimates of atmospheric SO_2 yield in order to investigate sulfur degassing mechanisms (Sharma et al., 2004; Sigmarsson et al., 2013). Depending on magma type, volcanic setting and eruption style, the atmospheric SO_2 yield retrieved from space can exceed the one resulting from the petrological estimates by up to one order of magnitude (Wallace 2001, Danyushevsky et al., 2002). For explosive eruptions, this behaviour, which is known as "excess SO_2", has been explained with the presence of a pre-eruptive exsolved SO_2 gas phase present at depth before the beginning of the eruption. From these analyses we can examine if excess SO_2 was produced during the Calbuco eruptions.

In the present work, major elements of Calbuco tephra samples were analysed using a JEOL JXA-8530F field emission Electron Microprobe Analyzer (EMPA) at the Photon Science Institute, University of Manchester (UK). Melt inclusions (MIs) in plagioclase phenocrysts and matrix glasses (gm) compositions were analysed using a 15 kV accelerating voltage, 10 nA beam current and beam size of 10 or 5 µm. Standard materials used for calibration were albite for Na; periclase for Mg; corundum for Al; fayalite for Fe; tephroite for Mn; apatite for P; sanidine for K; pyrite for S; halite for Cl; wollastonite for Ca and Si; and rutile for Ti. Sodium and potassium were measured first to minimize loss owing to volatilization. Futhermore, we used a secondary standard (Standard Glass Basalt, A-99) to have a double check on the quality of the analyses. The results obtained analysing the Basalt (A-99) support that Pyrite has been a reliable standard.

4 Results

4.1 Application of the Nnumerical Ttechnique to Calbuco Eeruptions

To investigate SO_2 plumes emitted during the Calbuco eruptions we use satellite data from the GOME-2 sensor (Rix et al., 2008). GOME-2 is an ultraviolet spectrometer (290-790 nm) aboard the polar-orbiting satellites MetOp-A (launched in 2006) and MetOp-B (launched in 2012) taking global measurements of atmospheric composition on daily basis. The two satellites operate in tandem with a temporal shift between acquisitions of 48 minutes and provide nadir-view scans with ground pixel size resolution equal to 40x40 km (swath of 960 km) in case of MetOp-A and 80x40 km (swath of 1920 km) in case of MetOp-B. ~~One of the most sensitive parameters influencing SO_2 vertical column amount as retrieved from space is plume altitude at the satellite measurement time. This data is an input parameter for the retrieval algorithms leading to vertical column estimation; however, it cannot be easily *a priori* assessed from space. In case of GOME-2, three vertical column densities are given for three hypothetical plume altitudes equal to 2.5 km, 6 km, 15 km.~~The Differential Optical Absorption Spectroscopy (DOAS) (Platt and Stutz, 2008) technique is applied to retrieve SO_2 vertical column amount by measuring the portion of the sunlight backscattered in the atmosphere. For GOME-2 retrievals, the overall error in SO_2 vertical column estimates is in the range 20-70% (Rix et al., 2012). This range of uncertainty accounts for both random and systematic errors. Random errors are mainly due to instrument noise and they are typically of 5-20%. The main contribution to systematic errors comes from the difficulty in assessing the plume height at measurement time and it is estimated to be in the range 10-60% (Rix et al., 2012). Plume height is a central parameter when converting SO_2 slant column density (i.e. the gas concentration along the entire light path) into vertical column density (i.e. the gas concentration right above the satellite footprint). When using an SO_2 retrieval done assuming the plume located at a certain height, errors up to 50% on vertical column amount can rise if the actual plume height is not the one used for the SO_2 retrieval. In order to deal with the missing information on plume height at measurement time, for GOME-2 retrievals, three different SO_2 estimates are given for three hypothetical plume altitudes equal to 2.5 km, 6 km, 15 km.

The first GOME-2 image of the Calbuco SO_2 plume was collected at ~13:00 on 23 April 2015, after the end of the two eruptive events. Then, plumes advection/dispersion paths can be followed for about one month until they are diluted under the satellite detection limit (GOME-2 images can be displayed and datasets downloaded from the Support to Aviation Control Service (SACS) website http://sacs.aeronomie.be/). Due to GOME-2 MetOpA and B different pixel resolution, the original image is re-gridded into a new one presenting a spatial resolution of 30x30 km. In Figure 2(a) we report atmospheric SO_2 loading in Dobson Unit (DU) retrieved assuming the plume located at 2.5 km with a spatial resolution of 30x30 km.

~~We used this dataset since, comparing it with the other retrievals (6 km and 15 km), we have an overestimation of the SO_2 atmospheric abundance and of its spatial distribution, ensuring, thus, that all the volcanic plume is considered in our model.~~As previously discussed, plume altitude is one of the main parameters influencing the retrieval of SO_2 vertical column amount. We use as an input image for our numerical procedure the SO_2 column amount image calculated assuming a plume height of 2.5 km. This means that the maximum accuracy in SO_2 estimation is achieved if the actual plume is located at 2.5 km. In case

of different plume height (higher than 2.5 km), SO_2 column amount for a single pixel can be overestimated up to 70-80% (Carn et al., 2013). On the contrary, when using the 6 and 15 km retrievals for a plume which is actually located at lower heights, the SO_2 column amount results to be underestimated and thus information on plume spatial distribution can be lost. Since we do not want to make assumptions on both plume height and SO_2 spatial distribution, we use as input data for our numerical model the SO_2 image at 2.5 km. In this way we operate our numerical procedure on a plume which is eventually broader than the actual one and we let the model retrieve the actual plume spatial distribution in term of SO_2 vertical column corrected for plume height.

In order to isolate volcanic plumes from background noise, we select pixels with a vertical column higher than a certain threshold (6 DU) calculated applied the Normalized Cloud-mass technique presented in Carn et al., (2008), see Figure 2(b). For our test case, the numerical wind data comes from the global ECMWF atmospheric reanalysis ERA Interim dataset with a 0.75° grid.

Since we do not ~~make~~ place initial ~~hypothesis~~ constraints on SO_2 plume altitude, and this information cannot be directly extrapolated from the satellite data, we initialize trajectories from 2 km (Calbuco altitude) to 30 km asl (upper stratosphere). Assuming an interval of 250 m between each starting height, we produce a total of 73 trajectories for each pixel. We set the centre position of each pixel as the starting point on the horizontal plane of each trajectory. The time at which the trajectories are initialized is coincident with the time at which the SO_2 vertical column was measured for each pixel.

After having reduced the number of possible trajectories going forward in time up to the time of acquisition of the 24 April image, we accept backward trajectories approaching Calbuco's vent location (41.33° S, 72.61° W) using Eq. (1) with the additional constraint from eruption time interval. This means that we consider as acceptable only backward trajectories approaching the vent at a time instant which is consistent with the eruption time interval. For the Calbuco eruptions, the eruption time is well constrained by visual-, satellite- and ground-based observations (SERNAGEOMIN 2015a, 2015b, 2015c; Van Eaton et al., 2016). Thus, for the study of Eruption 1, we use 21:00 and 22:30 UT (22 April) as beginning and end of the eruption, while 04:00 and 10:00 UT (23 April) are the values referred to Eruption2. It is the inclusion of accurate information on the timing of the eruption from independent observations which allows our approach to reveal details of the eruption evolution, and represents one of the main innovations of this work. The umbrella cloud radius $r(t)$ is evaluated every 10 min using the mass eruption rate (MER) for both Eruption 1 and Eruption 2. Since we do not have a precise estimation of mass eruption rates, we perform a sensitivity analysis on MER, investigating the range ($0.8 \cdot 10^6$ kg s^{-1} – $2.7 \cdot 10^7$ kg s^{-1}). These values are chosen accordingly to the minimum and maximum MER calculated for the 2015 Calbuco eruptions by previous works (Romero et al., 2016, Castruccio et al., 2016, Van Eaton et al., 2016). The sensitivity analysis is performed using the Design and Analysis toolKit for Optimization and Terascale (DAKOTA) (Adams et al., 2009), selecting a Latin Hypercube approach on a total number of 9 samples (i.e. 9 different values of MER). Therefore, for each MER and for each of the two eruptions, the umbrella cloud radius grows from 0 km (beginning of the eruption) to a maximum value (end~~ing~~ of the eruption), which depends on the MER . However, numerical results show that with the approaching condition expressed in Eq. (1) we do not have enough acceptable trajectories to cover most of the pixel in the computational domain. On the contrary, if we use a

fixed maximum approaching distance for Eruption 1 and Eq. (1) for Eruption 2, our results can cover most of the volcanic cloud. This is due to several uncertainties given by wind data, trajectory calculation and SO_2 spatial distribution captured by the satellite. An overall error in the range of 15-30% of the travel distance can be estimated for the trajectories computation. This error is due to computational inaccuracy, interpolation errors, starting position errors and wind field errors (Stohl 1998). Since our aim is to provide a good estimation of the SO_2 mass loading in the volcanic cloud, we prefer to consider a solution which cover most of the pixels in the computational domain. For this reason, for Eruption 1, we use a maximum approaching radius r = 280 km, whilst for Eruption 2 we calculate $r(t)$ every 10 minutes using Eq. (1). The maximum values for the umbrella radius computed at the end of Eruption 2 are 150 and 360 km for the two MER end members (respectively $0.8 \cdot 10^6$ kg s^{-1} and $2.7 \cdot 10^7$ kg s^{-1}). The sensitivity analysis performed on MER produces 9 sets of acceptable trajectories for each pixel (one set for each MER). For a given MER, the number of the acceptable trajectories can vary from 0 (i.e. no acceptable trajectories starting from the considered pixel) to 73 (i.e. all the trajectories starting from the considered pixel are acceptable).

4.2 Numerical Rresults

Using the previously described technique, we calculate the plume height, the injection height and the injection time for each pixel of the computational domain where SO_2 is detected. Figures 3 and 4 report both the mean values ($\bar{h}$, $\bar{h}_{vent}$ and $\bar{t}_{vent}$) and standard deviations (σ_h, $\sigma_{h_{vent}}$ and $\sigma_{t_{vent}}$) of plume parameters calculated for each pixel. Figure 3 shows the SO_2 cloud emitted from Eruption 1, whilst in Figure 4 we plot the one emitted from Eruption 2. We do not separate *a priori* the plume of Eruption 1 from the one that of Eruption 2, but it is the model that, according to the approaching time and radius, distinguishes the two plumes. Figures 3(a), (d) and 4(a), (d) show respectively $\bar{h}$ and σ_h computed for each pixel of the computational domain. Similarly, Figures 3(b), (e) and 4(b), (e) report $\bar{h}_{vent}$ and $\sigma_{h_{vent}}$ respectively, whereas Figures 3(c), (f) and 4(c), (f) illustrate $\bar{t}_{vent}$ and $\sigma_{t_{vent}}$.

As we can see from Figure 3 and 4, the whole SO_2 plume is split into two multi-layered clouds, both transported in the same direction (North North-East). The SO_2 injected into the atmosphere at the beginning of the eruptive phases travelled furthest from the vent, while pixels closer to vent location contain SO_2 emitted at the end of the two eruptions.

Due to low vertical velocity at stratospheric heights, $\bar{h}$ and $\bar{h}_{vent}$ are almost coincident (Figure 3(a), (b) and 4(a), (b)) and similar result is obtained for $\sigma_{h_{vent}}$ and σ_h (Figure 3(d), (e) and 4(d), (e)). SO_2 injected at the highest altitudes during Eruption 1 (from ~15 to 22 km) has been transported North-East, while SO_2 injected at lower altitudes (from ~11 to 15 km) has been mainly drifted North and it composes the tail of the plume. Moreover, a lower layer, below ~10 km, can be observed for the cloud related to produced by Eruption 1. The presence of this lower altitude layer is confirmed by the pictures of the Calbuco eruptive column taken during Eruption 1 (Romero et al., 2016; Castruccio et al., 2016) and from the analysis of the tephra deposit (Romero et al., 2016). This highlights the accuracy of our numerical technique in reproducing and unravelling the complex evolution of plume emission and dispersion. On the contrary, the SO_2 plume emitted during Eruption 2 (Figure 4) presents a more compact shape than the one of Eruption 1. A mean height of ~14 km both at vent and at satellite overpass is

computed, with peaks of ~18 km (Figure 4(a), (b)). For almost the whole cloud of Eruption 1, σ_h and $\sigma_{h_{vent}}$ are ~ 0.5 km (Figure 3(d), (e)), whilst for Eruption 2 are in the range 0-6 km with a mean value of 2 km (Figure 4(d), (e)). Finally, uncertainties on injection time ($\sigma_{t_{vent}}$) are 17 min and 45 min for Eruption 1 and Eruption 2 respectively (Figures 3(f) and 4(f)).

Our height retrievals appear to be consistent with those derived from analysis of both the tephra deposit and remote sensing techniques. Following the method of maximum clast diameters (Carey and Sparks, 1986), Romero et al., (2016) computed maximum column heights of 15.4 $\pm$ 3.08 km during Eruption 1 and the first phase of Eruption 2, while a decrease during the last phase of Eruption 2 emerges with heights of 12-13 km. Similar values are reported by Castruccio et al., (2016) with the only difference of proposing an increase in column height at the end the Eruption 2.

These values are also in agreement with ~~what~~ those presented by Van Eaton et al., (2016) considering the growth of the umbrella cloud (14.5-15.5 km for Eruption 1 and 16.9-17.3 km for Eruption 2). The main difference we notice from these ~~deposits~~ deposit-constrained estimates of plume height compared ~~to~~ with those ~~performed by~~ derived from our numerical simulation is the absence of heights higher than 20 km in the deposit-constrained data, probably because this material did not reach the ground. ~~However~~Indeed, Vidal et al., (2017) show, using a dual polarized weather radar, the main column located between 7 and 15 km for Eruption 2, with a maximum value of ~23 km asl, in agreement with our estimations for plume heights.

~~In Figure 5(a) we plot in red the pixels from which we have at least one acceptable trajectory for all the MER investigated, whilst in grey the pixels of the computational domain at satellite measurement time on 23 April 2015. As we can see, our numerical results cover most of the computational domain, even though we do not find any acceptable trajectory for the sparse pixels located in the northern region. From Figure 2(b) we can observe that the SO_2 column amount for these pixels is near to the chosen threshold, and their location is far from the main plume. Combining this information with our numerical results, we can conclude that SO_2 amount in these pixels is more likely to be associated with background noise rather than volcanic SO_2 emissions. In order to check the consistency of our numerical results, we perform a 24 h forward trajectory simulation initializing trajectories from the altitudes $h_f(i)$ from which we have found acceptable backward trajectories on the 23 April image. Figure 5(d) shows the comparison of our 24 h forward trajectory simulation with the volcanic SO_2 cloud taken from the 24 April satellite image (considering pixels with a vertical column higher than 6 DU), and a good match with the original image can be observed.~~ In order to test the consistency of our injection height time-series we perform forward trajectories simulations initialized from the values of $\bar{h}_{vent}$ and $\bar{t}_{vent}$ retrieved for each pixel. Trajectories endpoints are extracted in agreement with satellite measurement time on 24, 25 and 26 April 2015 as shown in Figure 5. Panels (a), (c) and (e) show GOME-2 images of the Calbuco plume, while in panels (b), (d) and (f) our forward trajectories simulations results are presented. A good match between the plume as captured by GOME-2 and as retrieved from our simulations can be observed. SO_2 located at higher altitudes (> 10 km) match well with the position of the plume as seen by GOME-2, while a discrepancy seems to emerge for the SO_2 travelling at lower heights. Deposition, dispersion and conversion processes affected atmospheric

SO_2 are possible sources of the mismatch between the satellite image and our retrieval on 26 April. This is due to the height-dependent SO_2 lifetime which is shorter (1-2 days) for tropospheric plumes than for stratospheric ones. Thus, SO_2 concentration on 26 April may have dropped under GOME-2 detection limit.

4.2.1 ~~Masses~~ Erupted gas and tephra mass estimations from numerical results and SO_2 flux time-series

SO_2 vertical columns retrieved from satellite data depend on several factors, such as plume height, SO_2 lifetime and satellite sensors signal saturation. SO_2 retrievals from GOME-2 report vertical columns for each pixel at 3 hypothetical plume heights of 2.5 km, 6 km, 15 km (Figure 6(a)-(c)). We interpolate SO_2 column amount between these three points and use our calculated mean SO_2 height ($\bar{h}$) to correct the column amount. In our test case, the effect related to SO_2 lifetime can be neglected. Indeed, lifetime of volcanic SO_2 injected into the stratosphere depends primarily on injection altitude, and can vary from 8-9 days for 11 km height plumes (Krotkov et al., 2010) to 25 days for higher injection altitudes (Guo et al., 2004). The brief time (<16 hours) between eruptions and satellite measurement means that SO_2 losses due to deposition or chemical conversion are not significant. Furthermore, we correct possible 30% underestimations of SO_2 loading due to signal saturation for vertical columns higher than 50-100 DU (Rix et al., 2008). Combining all of this information, we produce a corrected SO_2 column amount image for 2015 Calbuco eruptions (Figure 6(d)).

Comparing our height-corrected SO_2 column amounts with those retrieved from GOME-2, we see good agreement with satellite data between 6 km and 15 km. Mean square root errors computed from our numerical results and GOME-2 retrievals, reveal that the *a-priori* image which agrees best with our height-corrected SO_2 atmospheric loading is that assuming 15 km height. Mean square root errors are equal to 45.05 DU for the 2.5 km map, 12.51 DU and 8.75 DU for the 6 km and 15 km maps respectively.

We use the corrected SO_2 column amount to determine a total SO_2 mass loading of 300 ± 46 kt of SO_2 for the overall Calbuco eruptions, with 160 ± 30 kt produced by Eruption 1 and 140 ± 35 kt by Eruption 2. For each pixel of the computational domain we plot the retrieved SO_2 loading (kt) in Figure 7(a), (b). With contours we indicate mean altitudes at which SO_2 is located at satellite measurement time. During Eruption 1 the bulk of the SO_2 (83% of the total) was injected into the atmosphere in the range 8-16 km, while the remaining 17% was injected at heights ranging from 17-21 km (Figure 7(a)). On the contrary, Eruption 2 was characterized with 55% of the SO_2 injected at 15 km, 41% at 13 km and 4% at 3 km (Figure 7(b)).

Our retrieval of plume height time-series opens the possibility of quantifying mass eruption rate time-series, and to compare ~~these data~~ with field data. For the Calbuco eruptions, separation of volcanic ash and SO_2 gas has not been observed, so retrieved SO_2 injection heights are representative of column height evolution during the eruptions. Column height is primary controlled by the thermal buoyancy of the erupted material, which is a function of the mass flux supplied during the eruption (Sparks et al., 1997). We use our mean injection height time-series to calculate a mean mass eruption rate (MER) ~~every 10 minutes during the eruptions and we compute masses of erupted solid material by integrating MER over time.~~ and we use it to evaluate the mass of erupted solid material. From this calculation we compute a mean MER of $1.14\pm0.42\cdot10^7$ kg s^{-1} for Eruption 1 and of $1.09\pm0.38\cdot10^7$ kg s^{-1} for Eruption 2 and ~~We~~ we infer ~~$9\cdot10^4$ kt~~ $6.2\pm2.2\cdot10^4$ kt emitted during Eruption 1 and ~~$25\cdot10^4$ kt~~

24±8.2·10^4 kt during Eruption 2. These values are in good agreement with those from Castruccio et al., (2016) which report 8·10^4 kt for Eruption 1 and 32·10^4 kt for Eruption 2. Our satellite-based interpretation seems to confirm the eruptive scenario proposed by Castruccio et al., (2016) which assign the first ~~or~~ of the four layers of the deposit to the first eruption and the other three to the second one. Differently, Romero et al., (2016) assign the first two layers to Eruption 1 and the other two to Eruption 2.~~,~~ ~~despite~~ Despite this, the two authors agree on the general stratigraphy.

~~With~~ Assuming a magma density of ~2500 kg m^{-3}~~for the whole deposit~~, we compute a deposit dense rock equivalent (DRE) of ~~0.136~~0.122±0.030 km^3, with ~~0.036~~0.025±0.009 km^3 resulting from Eruption 1 and ~~0.1~~0.096±0.03 km^3 from Eruption 2. For Eruption 1 a magma volume of ~ 0.~~036~~025 km^3 produced ~ 0.16 Mt of SO_2, while ~ 0.~~1~~096 km^3 of magma produced ~ 0.14 Mt of SO_2 for Eruption 2. Thus, Eruption 1 produced about one order of magnitude excess SO_2 per unit mass erupted than Eruption 2.

Finally, by associating the injection time at the vent (t_{vent}) for each pixel SO_2 mass loading we calculate SO_2 flux time-series (Figure 8(a)). The similar amount of SO_2 released during the two eruptions and the different duration of the events (1.5 h and 6 h) are reflected in the average SO_2 fluxes. Eruption 1 produced an intense gas emission with mean flux of 2560 kt day^{-1}, while a smoother Gaussian shape curve can be observed for Eruption 2 together with a much lower mean flux of 560 kt day^{-1}. SO_2 flux ~~is well correlated~~ appears to be ~~with~~correlated with mean injection heights for both eruptions (Figure 8(b)). Comparing SO_2 flux and injection height time-series, two different volcanic processes driving Eruption 1 and 2 emerge. This is reflected in the similar total amount of SO_2 (~150 kt) released in different time scale (1.5 h and 6 h) but in a similar range of altitudes (13-15 km), see the Discussion.

4.3 Petrological Results

The scoriae erupted from Calbuco contain plagioclase, orthopyroxene and clinopyroxene phenocrysts and a variably crystallised groundmass with microlites of plagioclase, pyroxene and patches of glass. Melt inclusions (MIs) are hosted in plagioclase phenocrysts and they are characterized by spherical to oblate shape. Their size range from 30 to 100 μm. The composition of MIs is andesitic, groundmass glass composition is andesitic-dacitic (see Supplementary Table 1).

Data obtained from melt inclusions may be complicated by either post-entrapment effects and the fact that inclusions may be trapped after some degassing of melt has already occurred (Lowenstern 1995; Métrich and Wallace 2008). In fact, our MIs hosted in plagioclase may not represent the initial sulfur concentration in the melt before crystallization of the magma. The bulk composition of Calbuco rocks is a basaltic-andesite (Romero et al., 2016; Castruccio et al., 2016), whereas MIs have an andesitic composition. The difference in composition between the original melt (basaltic-andesite) and erupted glasses (andesite) is consistent with fractional crystallization, which would produce exsolution of volatiles, Figure 9. This means that the sulfur concentration in the MIs may be a little bit lower than the one dissolved in the basaltic-andesitic melt since part of the originally dissolved sulfur has been exsolved due to crystallization. Post-entrapment crystallization is evident in some MIs, but we have analysed only glassy MIs avoiding crystallized MIs. Furthermore, MIs and residual melt have similar K_2O concentration, whereas sulfur concentration decreases in the residual melt indicating that sulfur degassing occurred in syn-

eruptive conditions (in agreement with Sigmarsson et al., (2013)),see Figure 9(a). MIs have also higher MgO than matrix glass, due to the crystallization of microlites of orthopyroxene in the ground mass rather than post-entrapment crystallization in MIs, Figure 9(b). Therefore, we have not performed any post-entrapment crystallisation corrections on our MI compositions.

According to Castruccio et al., (2016), we consider scoriae of the first layer (layer A) as produced by Eruption 1 and those from the other three layers (layers B, C and D) from Eruption 2. Sulfur concentrations in the MIs of Eruption 1 (scoriae of layer A) vary from 240 to 520 ppm (Supplementary Table 1), and sulfur contents in the MIs of Eruption 2 (scoriae of layers B, C and D) ranges between 270 and 590 ppm. Low values of sulfur are measured in the matrix glasses of the scoriae erupted from both eruptions, ranging between 30 and 150 ppm (these values are close to the detection limit of the electron microprobe, see Supplementary Table 1). The mean sulfur content in the andesitic melt at pre-eruptive conditions is equal to 350 ppm for Eruption 1 and 400 ppm for Eruption 2, whereas, the residual andesitic-dacitic melt was practically devoid of sulfur (<100 ppm), see Table 1.

In order to evaluate the atmospheric SO_2 yield as shown in Eq. (8), we consider a crystal fraction of 50 vol% (i.e. CF equal to 0.5 (Arzilli et al., (2017)). For Eruption 1 M, S_{MI} and S_{gm} are equal to 6.2±2.2·10^4 kt, 0.035±0.01 wt% and 0.009±0.0006 wt%, while for Eruption 2 they are equal to 24±8.2·10^4 kt, 0.04±0.007 wt% and 0.01±0.003 wt%, Table1. From Eq.(8), the SO_2 yield emitted during Eruption 1 is 16±7 kt, while the one emitted during Eruption 2 is 71±26 kt, see $m(SO_2)_{PETR}$ in Table1.

5. Discussion

We found that the SO_2 emitted per km^3 of erupted ~~lavas~~ products during Eruption 1 ~~was~~ is about one order of magnitude higher than that of Eruption 2, and this indicates a major difference in the style of the two eruptive events, with a key role for excess SO_2 in Eruption 1. Excess SO_2 has been invoked to explain a large body of evidence where satellite detection of volcanic SO_2 plumes demonstrated that the amount of SO_2 released into the atmosphere during volcanic eruptions, both explosive and effusive, can exceed that resulting from syneruptive volatile exsolution (Devine et al., 1984). Wallace (2001) shows that there is a fixed ratio between the volume of erupted magma (expressed in km^3) and the SO_2 loading (expressed in Mt) which is released due to syneruptive degassing of erupted magma. In particular, for an andesite magma, the ratio between these two quantities is typically ~1 Mt km^{-3}. However, in some cases, the SO_2 emitted is higher than that which can be produced by syneruptive degassing. This means that the SO_2 released into the atmosphere during an eruption is the sum of two contributions. The first is the SO_2 derived from syneruptive degassing of erupted magma, while the second is the SO_2 derived from a pre-existing exsolved gas phase present inside the magma chamber before the eruption starts. The process which produces such excess SO_2 depend on tectonic setting, magma type, magma evolution and eruption style (Shinohara 2008). However, excess SO_2 appears to be particularly characteristic of explosive eruptions of intermediate and silicic magma in subduction zone settings (Andres et al., 1991), such as Calbuco.

Romero et al., (2016) show that the 2015 Calbuco eruptions were fed by a basaltic-andesitic magma (~55 wt.% of SiO_2), and therefore the ratio between the SO_2 emitted and the volume of magma erupted might be expected to be close to ~1 Mt km^{-3}.

Our results ~~for Eruption 2 are consistent with the relation showed by Wallace (2001)~~ show a ratio of 7.0±2.7 Mt km^{-3} for Eruption 1 and 1.58±0.6 Mt km^{-3} for Eruption 2. ~~However, for Eruption 1, the ratio between the SO_2 released and the volume ejected is ~5 Mt km^{-3}.~~ This ~~clearly~~ suggests ~~that, prior to Eruption 1, there was already an exsolved volatile phase in the magma chamber.~~ the presence of excess SO_2 for both the events, with Eruption 1 presenting a higher content of pre-eruptive exsolved SO_2 than Eruption 2.

~~For sub-Plinian eruptions like Calbuco 2015 the most likely mechanism responsible for excess SO_2 is pre-eruptive exsolution of volatiles supplied from deeper magma Wallace 2001; Shinohara 2008. Due to buoyancy forces, bubbles migrated at the top of the magma chamber, forming a gas-rich cupola.~~ We suggest that the overpressure resulting from excess volatiles (possibly also H_2O and CO_2 (Wallace 2005; Edmonds et al., 2010)) into the magma chamber may ~~this deep exsolution may~~ have ~~also~~ provided the trigger for the eruptions onset. ~~During the course of Eruption 1, all the pre-existing volatile phase was ejected into the atmosphere. However, the short repose time between the two eruptions was not enough to accumulate significant amounts of gas from deeper magma. Thus, we can infer that Eruption 2 was driven mainly by syneruptive volatile exsolution without the presence of a volatile excess from depth.~~

In order to test ~~this~~ the hypothesis of a pre-accumulated gas phase powering ~~Eruption 1~~the eruptions, ~~and a simple syneruptive magma ascent sustaining Eruption 2,~~ we ~~performed electron microprobe analyses (technical details are reported in the Supplementary Materials) on the erupted products of both eruptions, to derive SO_2 mass loss in both eruptions. In detail, the scoriae erupted from Calbuco contain plagioclase, orthopyroxene and clinopyroxene as phenocrysts and a crystallised groundmass with patches of glass. Melt inclusions (MIs) are hosted in plagioclase phenocrysts and they are characterized by spherical to oblate shape. Sizes of MIs range from 30 to 300 μm. The groundmass is composed of glass patches with variable microlite contents ranging from lowly to heavily crystallized groundmass. The composition of MIs is andesitic, instead the groundmass glass composition is andesitic-dacitic (see Supplementary Materials). According to electron microprobe analyses, differences between sulfur contents of glassy melt inclusions (S_{MI}) and matrix glasses (S_{gm}) scaled to masses of erupted solid material provide estimates of minimum sulfur yield to the atmosphere during an eruption. In order to compare our satellite estimates of SO_2 mass loadings with elemental sulfur concentrations measured from microprobe analyses, its useful to convert sulfur mass loadings into SO_2 mass loadings, which is readily achieved by multiplying by two, following the molecular weight of SO_2 (64 g mol^{-1}) and atomic weight of sulfur (32 g mol^{-1}), see $m(SO_2)_{PETR}$ column in Table1. From the petrological method we infer 38±12 kt and 120±26 kt of SO_2 emitted during Eruption 1 and 2 respectively. Comparing masses of~~compare the SO_2 yield derived from our numerical satellite-based technique, with ~~those~~ the one resulting from ~~microprobe analyses~~ petrological estimates, and we calculate the excess SO_2 (Devine et al., 1984). We evaluate the excess SO_2 as the difference between the mass of SO_2 inferred from space and the one inferred from the petrological analysis, $m(SO_2)_{SAT}$ and $m(SO_2)_{PETR}$ in Table1. For Eruption 1, we found ~~122~~144±2~~6~~8 kt of excess SO_2, whereas for Eruption 2 ~~jus~~t ~~20~~69±3~~9~~8 kt, see $m(SO_2)_{ex}$ of Table 1. This demonstrates that ~~about the~~ 90±20 ~~76~~% of the SO_2 emitted during Eruption 1 and 49±30 % of SO_2 emitted during Eruption 2 were~~as~~ already present as part of the pre-eruptive exsolved gas phase, in agreement with our hypothesis. ~~Instead, for Eruption~~

~~2 there is, within error limits, no excess SO_2.~~ Thus, the combined satellite and petrological analysis confirms our original hypothesis for a key role for excess SO_2 based purely from satellite data.

6 Conclusions

We have developed a new technique to retrieve SO_2 flux time-series and eruption plume height at high spatial resolution (30 km) and high time resolution (10 minutes). Our numerical procedure, which combines satellite imagery of volcanic SO_2 plumes with independent observations of the timing of the eruption and forward and backward trajectory simulations, can be generally applied, and used to investigate SO_2 emission during any type of volcanic eruption. The algorithm is computationally efficient, and can be run in an automated manner on a standard PC in <12 hours. Retrieved plume heights are used to correct the assumption that the whole plume is located at the same hypothetical altitude, thus producing corrected SO_2 ~~columnar~~ column amount maps.

~~Here, we quantified SO_2 emissions from the recent April 2015 Calbuco eruptions using imagery from the GOME-2 satellite sensor.~~ We applied this new algorithm to GOME-2 satellite imagery of plumes produced during the April 2015 Calbuco eruptions. We retrieved ~~both~~ SO_2 injection height and flux time-series together with masses of erupted material and we used them to unravel triggering mechanisms and volcanic processes of the Calbuco eruptions. ~~We found excellent agreement between the integrated mass eruption rates inferred from plume height time series and field studies of the eruption deposit masses. Furthermore, our results highlight the presence of different exsolved volatile phase at depth between the two eruptions.~~ Comparing our results in terms of atmospheric SO_2 yield and masses of solid material released during the eruptions, we inferred the presence of different exsolved volatile phase at depth between the two eruptions. Indeed, Eruption 1 appears to be richer in pre-eruptive exsolved SO_2 than Eruption 2. Electron microprobe analyses performed on Calbuco tephra samples confirmed our conclusions, validating our hypothesis made just from our numerical technique.~~Thanks to the quantitative comparison of SO_2 flux and plume height time-series, we infer the presence of excess SO_2 in Eruption 1.~~ From satellite and petrological analyses, ~~We~~we found that at least ~~76~~90% of total SO_2 emitted in Eruption 1 was sourced from pre-eruptive volatile exsolution possibly due to magma crystallization. ~~We suggest that bubbles migrated to the top of the magma chamber forming a gas-rich cupola. The overpressure caused by this gas accumulation could have played a key role in triggering Eruption 1. On the other hand,~~ For Eruption 2 we found that the amount of pre-eruptive exsolved SO_2 is equal to the ~50% of the overall SO_2 released, meaning that Eruption 2 was fed by a lower content of pre-eruptive exsolved SO_2 in compare to Eruption 1. One of the main results of this study is the evidence that exsolved SO_2 was present before the onset of the eruptions, highlighting that other volatiles (H_2O, CO_2 and Cl) were already exsolved at the same pre-eruptive conditions (Wallace 2005; Edmonds et al., 2010). This lead us to conclude that the overpressure due to pre-eruptive exsolved volatiles (not only SO_2, but probably also H_2O and CO_2) may have played a role in the triggering mechanisms of both the sub-Plinian eruptions.

~~swas consistent with a syneruptive degassing, since no excess SO_2 was observed. Electron microprobe analyses performed on Calbuco samples confirmed our conclusions, validating our hypothesis made just from our numerical technique.~~

This work highlights the capability of trajectory analysis of satellite SO_2 imagery to extract SO_2 height and flux time-series and reveal sub-surface magmatic processes. We highlight that plotting time-series of retrieved SO_2 flux against retrieved plume heights is an effective tool to examine patterns in eruption processes, the role of excess SO_2 degassing, and comparinge eruptions. Our approach could be applied to the reanalysis of SO_2 imagery collected during past volcanic eruptions. This opens the possibility of a database that would be a powerful tool for real time analysis of satellite data collected during an eruption. Indeed, satellite images of volcanic SO_2 plumes are available in almost real time when an eruption occurs and they could be used not only for aviation safety mitigation but also for operational monitoring of subsurface processes especially in conjunction with other geophysical data. These data may greatly help the quantification of stratospheric mass loadings of SO_2, which can impact global temperatures through the formation of ~~sulphuric~~ sulfuric acid aerosols (Kirchner et al., 1999), and mass loadings of HCl, using either assumptions or measurements of SO_2/HCl masses, and these could be invaluable in the determination of ozone depletion processes (Solomon et al., 2016; Ivy et al., 2017).

References

Adams, B. M., Bohnhoff, W. J., Dalbey, K. R., Eddy, J. P., Eldred, M. S., Gay, D. M., Haskell, K., Hough, P. D. and Swiler, L. P.: DAKOTA, a multilevel parallel object-oriented framework for design optimization, parameter estimation, uncertainty quantification, and sensitivity analysis: version 5.0 user's manual, Sandia National Laboratories, Tech. Rep. SAND2010-2183, doi:DOI: 10.2172/991842, 2009.

Andres, R. J., Rose, W. I., Kyle, P. R., DeSilva, S., Francis, P., Gardeweg, M. and Roa, H. M.: Excessive sulfur dioxide emissions from Chilean volcanoes. Journal of Volcanology and Geothermal Research, 46(3-4), pp.323-329, 1991.

Arzilli, F., Morgavi, D., Petrelli, M., Polacci, M., Burton, M., Di Genova, D., Spina, L., La Spina, G., Hartley, M., Romero, J.E., Fellowes, J., Alvarado J.D and Perugini D.: Self triggered sub-Plinian eruptions: Calbuco volcano (22–23 April 2015, southern Chile), 2017. (In preparation).

Bègue, N., Vignelles, D., Berthet, G., Portafaix, T., Payen, G., Jégou, F., Benchérif, H., Jumelet, J., Vernier, J.-P., Lurton, T., Renard, J.-B., Clarisse, L., Duverger, V., Posny, F., Metzger, J.-M., and Godin-Beekmann, S.: Long-range isentropic transport of stratospheric aerosols over Southern Hemisphere following the Calbuco eruption in April 2015, Atmos. Chem. Phys. Discuss., https://doi.org/10.5194/acp-2017-544, in review, 2017.

Boichu, M., Menut, L., Khvorostyanov, D., Clarisse, L., Clerbaux, C., Turquety, S. and Coheur, P.-F.: Inverting for volcanic SO_2 flux at high temporal resolution using spaceborne plume imagery and chemistry-transport modelling: the 2010 Eyjafjallajökull eruption case-study, Atmospheric Chemistry and Physics, 13(17), 8569–8584, doi:10.5194/acp-13-8569-2013, 2013.

Brenot, H., Theys, N., Clarisse, L., Van Geffen, J., Van Gent, J., Van Roozendael, M., Van Der A, R., Hurtmans, D., Coheur, P.-F. and Clerbaux, C.: Support to Aviation Control Service (SACS): an online service for near real-time satellite monitoring of volcanic plumes, Natural hazards and earth system sciences, 14(5), 1099–1123, doi:10.5194/nhess-14-1099-2014, 2014.

Campion, R.: New lava lake at Nyamuragira volcano revealed by combined ASTER and OMI SO2 measurements, Geophys. Res. Lett., 41, 7485–7492, doi:10.1002/2014GL061808, 2014.

Carboni, E., Grainger, R., Walker, J., Dudhia, A. and Siddans, R.: A new scheme for sulphur dioxide retrieval from IASI measurements: application to the Eyjafjallajökull eruption of April and May 2010, Atmospheric Chemistry and Physics, 12(23), 11417–11434, ~~doi:~~doi:10.5194/acp-12-11417-2012, 2012.

Carboni, E., Grainger, R. G., Mather, T. A., Pyle, D. M., Thomas, G. E., Siddans, R., Smith, A. J. A., Dudhia, A., Koukouli, M. E., and Balis, D.: The vertical distribution of volcanic SO_2 plumes measured by IASI, Atmos. Chem. Phys., 16, 4343-4367, https://doi.org/10.5194/acp-16-4343-2016, 2016.

Carey, S. and Sparks, R. S. J.: Quantitative models of the fallout and dispersal of tephra from volcanic eruption columns, Bulletin of Volcanology, 48(2), 109–125, doi:10.1007/BF01046546, 1986.

Carn, S. A., Krueger, A. J., Arellano, S., Krotkov, N. A. and Yang, K.: Daily monitoring of Ecuadorian volcanic degassing from space, Journal of Volcanology and Geothermal Research, 176(1), 141–150, doi:10.1016/j.jvolgeores.2008.01.029, 2008.

Carn, S. A., and Prata F. J.: Satellite-based constraints on explosive SO_2 release from Soufrière Hills Volcano, Montserrat, Geophys. Res. Lett., 37, L00E22, doi:10.1029/2010GL044971, 2010.

Carn, S. A., Krotkov, N. A., Yang, K., and Krueger, A. J.: Measuring global volcanic degassing with the Ozone Monitoring Instrument (OMI), Geological Society, London, Special Publications, 380, 229–257, doi: 10.1144/SP380.12, 2013.

Carn, S. A., Clarisse, L., and Prata, A. J.: Multi-decadal satellite measurements of global volcanic degassing, Journal of Volcanology and Geothermal Research, 311, 99-134, 10.1016/j.jvolgeores.2016.01.002, 2016.

Castruccio, A., Clavero, J., Segura, A., Samaniego, P., Roche, O., Le Pennec, J.-L. and Droguett, B.: Eruptive parameters and dynamics of the April 2015 sub-Plinian eruptions of Calbuco volcano (southern Chile), Bulletin of Volcanology, 78(9), 62, doi:10.1007/s00445-016-1058-8, 2016.

Clarisse, L., Coheur, P.-F., Chefdeville, S., Lacour, J.-L., Hurtmans, D. and Clerbaux, C.: Infrared satellite observations of hydrogen sulfide in the volcanic plume of the August 2008 Kasatochi eruption, Geophysical research letters, 38(10),

doi:10.1029/2011GL047402, 2011.

Clarisse, L., Coheur, P.-F., Theys, N., Hurtmans, D. and Clerbaux, C.: The 2011 Nabro eruption, a SO_2 plume height analysis using IASI measurements, Atmospheric chemistry and physics, 14(6), 3095–3111, doi:10.5194/acp-14-3095-2014, 2014.

Danyushevsky, L.V., McNeill, A.W. and Sobolev, A.V.: Experimental and petrological studies of melt inclusions in phenocrysts from mantle-derived magmas: an overview of techniques, advantages and complications. Chemical Geology, 183(1), pp.5-24, 2002.

Devine, J. D., Sigurdsson, H., Davis, A. N. and Self, S.: Estimates of sulfur and chlorine yield to the atmosphere from volcanic eruptions and potential climatic effects, Journal of Geophysical Research: Solid Earth, 89(B7), 6309–6325, doi:10.1029/JB089iB07p06309, 1984.

Eckhardt, S., Prata, A. J., Seibert, P., Stebel, K. and Stohl, A.: Estimation of the vertical profile of sulfur dioxide injection into the atmosphere by a volcanic eruption using satellite column measurements and inverse transport modeling, Atmospheric Chemistry and Physics, 8(14), 3881–3897, doi:doi:10.5194/acp-8-3881-2008, 2008.

Edmonds, M., Aiuppa, A., Humphreys, M., Moretti, R., Giudice, G., Martin, R. S., Herd, R. A., Christopher, T.: Excess volatiles supplied by mingling of mafic magma at an andesite arc volcano, Geochem. Geophys. Geosyst., 11, Q04005, doi:10.1029/2009GC002781, 2010.

Grainger, R. G., Mather, T. A., Pyle, D. M., Thomas, G. E., Smith, A. J. and Koukouli, M. E.: The vertical distribution of volcanic SO_2 plumes measured by IASI, Atmospheric Chemistry and Physics, 16(7), 4343, doi:10.5194/acp-16-4343-2016, 2016.

Guo, S., Bluth, G. J., Rose, W. I., Watson, I. M. and Prata, A. J.: Re-evaluation of SO_2 release of the 15 June 1991 Pinatubo eruption using ultraviolet and infrared satellite sensors, Geochemistry, Geophysics, Geosystems, 5(4), doi:10.1029/2003GC000654, 2004.

Hayer, C. S., Wadge, G., Edmonds, M. and Christopher, T.: Sensitivity of OMI SO_2 measurements to variable eruptive behaviour at Soufrière Hills Volcano, Montserrat, Journal of Volcanology and Geothermal Research, 312, 1–10, doi:doi.org/10.1016/j.jvolgeores.2016.01.014, 2016.

Heng, Y., L. Hoffmann, S. Griessbach, T. Rößler, and O. Stein: Inverse transport modeling of volcanic sulfur dioxide emissions using large-scale simulations, Geosci. Model Dev., 9, 1927–1645, doi:10.5194/gmd-9-1627-2016, 2016.

Hughes, E. J., Sparling, L. C., Carn, S. A. and Krueger, A. J.: Using horizontal transport characteristics to infer an emission

height time series of volcanic SO_2, Journal of Geophysical Research: Atmospheres, 117(D18), doi:10.1029/2012JD017957, 2012.

Ivy, D. J., Solomon, S., Kinnison, D., Mills, M. J., Schmidt, A. and Neely, R. R.: The influence of the Calbuco eruption on the 2015 Antarctic ozone hole in a fully coupled chemistry-climate model, Geophysical Research Letters, 44(5), 2556–2561, doi:10.1002/2016GL071925, 2017.

Kirchner, I., G. Stenchikov, H.-F. Graf, A. Robock. J. Antuna, Climate model simulation of winter warming and summer cooling following the 1991 Mount Pinatubo volcanic eruption, J. Geophys. Res., 104, 19,039-19,055, 1999.

Krotkov, N. A., Schoeberl, M. R., Morris, G. A., Carn, S. and Yang, K.: Dispersion and lifetime of the SO_2 cloud from the August 2008 Kasatochi eruption, Journal of Geophysical Research: Atmospheres, 115(D2), doi:10.1029/2010JD013984, 2010.

Krueger, A. J., Schnetzler, C. C. and Walter, L. S.: The December 1981 eruption of Nyamuragira volcano (Zaire), and the origin of the "mystery cloud" of early 1982, Journal of Geophysical Research: Atmospheres, 101(D10), 15191–15196, doi:10.1029/96JD00221, 1996.

Lopez, T., Carn, S., Werner, C., Fee, D., Kelly, P., Doukas, M., Pfeffer, M., Webley, P., Cahill, C. and Schneider, D.: Evaluation of Redoubt Volcano's sulfur dioxide emissions by the Ozone Monitoring Instrument, Journal of Volcanology and Geothermal Research, 259, 290–307, doi:10.1016/j.jvolgeores.2012.03.002, 2013.

Lopez-Escobar, L., Parada, M. A., Moreno, H., Frey, F. A. and Hickey-Vargas, R. L.: A contribution to the petrogenesis of Osomo and Calbuco volcanoes, Southern Andes (41° 00'-41° 30'S): comparative study, Andean Geology, 19(2), 211–226, doi:http://dx.doi.org/10.5027/andgeoV19n2-a05, 1992.

Lowenstern, J. B.: Applications of silicate melt inclusions to the study of magmatic volatiles. In: Thompson JFH (ed) Magmas, Fluids, and Ore Deposits. Miner. Assoc. Canada Short Course 23:71–99, 1995.

McCormick, B. T., Herzog, M., Yang, J., Edmonds, M., Mather, T. A., Carn, S. A., Hidalgo, S. and Langmann, B.: A comparison of satellite-and ground-based measurements of SO_2 emissions from Tungurahua volcano, Ecuador, Journal of Geophysical Research: Atmospheres, 119(7), 4264–4285, doi:10.1002/2013JD019771, 2014.

Merucci, L., Burton, M., Corradini, S. and Salerno, G. G.: Reconstruction of SO_2 flux emission chronology from space-based measurements, Journal of Volcanology and Geothermal Research, 206(3), 80–87, doi:10.1016/j.jvolgeores.2011.07.002, 2011.

Métrich N., Wallace P.: Volatile abundances in basaltic magmas and their degassing paths tracked by melt inclusions. In:Minerals, Inclusions & Volcanic Processes, (eds K. Putirka& F. Tepley). Rev. Mineral. Geochem., 69, Chapter 10, pp. 363-

402, 2008.

Moxnes, E. D., Kristiansen, N. I., Stohl, A,. Clarisse, L., Durant, A., Weber, K., Vogel, A.: Separation of ash and sulfur dioxide during the 2011 Grímsvötn eruption, J. Geophys. Res. Atmos., 119, 7477–7501, doi:10.1002/2013JD021129, 2014.

Nowlan, C. R., Liu, X., Chance, K., Cai, Z., Kurosu, T. P., Lee, C., Martin, R. V.: Retrievals of sulfur dioxide from the Global Ozone Monitoring Experiment 2 (GOME-2) using an optimal estimation approach: Algorithm and initial validation, J. Geophys. Res., 116, D18301, doi:10.1029/2011JD015808, 2011.

Oppenheimer, C., Scaillet, B. and Martin, R. S.: Sulfur degassing from volcanoes: source conditions, surveillance, plume chemistry and earth system impacts, Reviews in Mineralogy and Geochemistry, 73(1), 363–421, doi:10.2138/rmg.2011.73.13, 2011.

Platt U., Stutz J.: Differential Absorption Spectroscopy. In: Differential Optical Absorption Spectroscopy. Physics of Earth and Space Environments. Springer, Berlin, Heidelberg, 2008.

Pardini, F., Burton, M., Vitturi, M. de'Michieli, Corradini, S., Salerno, G., Merucci, L. and Di Grazia, G.: Retrieval and intercomparison of volcanic SO_2 injection height and eruption time from satellite maps and ground-based observations, Journal of Volcanology and Geothermal Research, 331, 79–91, doi:10.1016/j.jvolgeores.2016.12.008, 2017.

Rix, M., Valks, P., Hao, N., Erbertseder, T. and Van Geffen, J.: Monitoring of volcanic SO_2 emissions using the GOME-2 satellite instrument, in Use of Remote Sensing Techniques for Monitoring Volcanoes and Seismogenic Areas, 2008. USEReST 2008. Second Workshop on, pp. 1–5, IEEE., 2008.

Rix, M., Valks, P., Hao, N., Loyola, D., Schlager, H., Huntrieser, H., Flemming, J., Koehler, U., Schumann, U. and Inness, A.: Volcanic SO_2, BrO and plume height estimations using GOME-2 satellite measurements during the eruption of Eyjafjallajökull in May 2010, Journal of Geophysical Research: Atmospheres, 117(D20), doi:10.1029/2011JD016718, 2012.

Romero, J. E., Morgavi, D., Arzilli, F., Daga, R., Caselli, A., Reckziegel, F., Viramonte, J., Díaz-Alvarado, J., Polacci, M. and Burton, M.: Eruption dynamics of the 22–23 April 2015 Calbuco volcano (Southern Chile): Analyses of tephra fall deposits, Journal of Volcanology and Geothermal Research, 317, 15–29, doi:10.1016/j.jvolgeores.2016.02.027, 2016.

SERNAGEOMIN, 2015a. Reporte Especial de Actividad Volcánica (REAV) Región de los Lagos. (REAV) Año 2015 Abril 22 (20:45 HL).

SERNAGEOMIN, 2015b. Reporte Especial de Actividad Volcánica (REAV) Región de los Lagos. Año 2015 Abril 22 (22:30 HL).

SERNAGEOMIN, 2015c. Reporte Especial de Actividad Volcánica (REAV) Región de los Lagos. Año 2015 Abril 23 (10:30 HL)

Sharma, K., Blake, S., Self, S., Krueger, A. J.: SO2 emissions from basaltic eruptions, and the excess sulfur issue, Geophys. Res. Lett., 31, L13612, doi:10.1029/2004GL019688, 2004.

Shinohara, H.: Excess degassing from volcanoes and its role on eruptive and intrusive activity, Reviews of Geophysics, 46(4), doi:10.1029/2007RG000244, 2008.

Sigmarsson, O., B. Haddadi, S. Carn, S. Moune, J. Gudnason, K. Yang, and L. Clarisse: The sulfur budget of the 2011 Grímsvötn eruption, Iceland, Geophys. Res. Lett., 40, 6095–6100, doi:10.1002/2013GL057760, 2013.

Solomon, S., Ivy, D.J., Kinnison, D., Mills, M.J., Neely, R.R. and Schmidt, A. Emergence of healing in the Antarctic ozone layer. Science, 353(6296), pp.269-274, 2016.

Sparks, R. S. J.: M. 1. Bursik, SN Carey, JS Gilbert, LS Glaze, H. Sigurdsson and AW Woods. Volcanic Plumes, Wiley: New York., 1997.

Stein, A. F., Draxler, R. R., Rolph, G. D., Stunder, B. J., Cohen, M. D. and Ngan, F.: NOAA's HYSPLIT atmospheric transport and dispersion modeling system, Bulletin of the American Meteorological Society, 96(12), 2059–2077, doi:10.1175/BAMS-D-14-00110.1, 2015.

Stohl, A.: Computation, accuracy and applications of trajectories – a review and bibliography, Atmos. Environ., 32, 947–966, 1998.

Textor, C., Graf, H.-F., Timmreck, C. and Robock, A.: Emissions from volcanoes, in Emissions of Atmospheric Trace Compounds, pp. 269–303, Springer., 2004.

Theys, N., Campion, R., Clarisse, L., van Gent, J., Dils, B., Corradini, S., Merucci, L., Coheur, P. F., Van Roozendael, M. and Hurtmans, D.: Volcanic SO_2 fluxes derived from satellite data: a survey using OMI, GOME-2, IASI and MODIS, Atmospheric Chemistry and Physics (ACP), doi:10.5194/acp-13-5945-2013, 2013.

Van Eaton, A. R., Amigo, Á., Bertin, D., Mastin, L. G., Giacosa, R. E., González, J., Valderrama, O., Fontijn, K. and Behnke, S. A.: Volcanic lightning and plume behavior reveal evolving hazards during the April 2015 eruption of Calbuco volcano, Chile, Geophysical Research Letters, 43(7), 3563–3571, doi:10.1002/2016GL068076, 2016.

Vidal, L., Nesbitt, S. W., Salio, P., Farias, C., Nicora, M. G., Osores, M. S., Mereu, L. and Marzano, F. S.: C-band Dual-Polarization Radar Observations of a Massive Volcanic Eruption in South America, IEEE Journal of Selected Topics in Applied Earth Observations and Remote Sensing, 10(3), 960–974, doi:DOI: 10.1109/JSTARS.2016.2640227, 2017.

Wallace, P. J.: Volcanic SO_2 emissions and the abundance and distribution of exsolved gas in magma bodies, Journal of Volcanology and Geothermal Research, 108(1), 85–106, doi:10.1016/S0377-0273(00)00279-1, 2001.

Wallace, P.J.: Volatiles in subduction zone magmas: concentrations and fluxes based on melt inclusion and volcanic gas data. Journal of Volcanology and Geothermal Research, 140(1), pp.217-240, 2005.

Wallace, P.J. and Edmonds, M.: The sulfur budget in magmas: evidence from melt inclusions, submarine glasses, and volcanic gas emissions. Reviews in Mineralogy and Geochemistry, 73(1), pp.215-246, 2011.

Westrich, H. R. and Gerlach, T. M.: Magmatic gas source for the stratospheric SO_2 cloud from the June 15, 1991, eruption of Mount Pinatubo, Geology, 20(10), 867–870, doi:10.1130/0091-7613(1992) 020<0867:MGSFTS>2.3., 1992.

~~Wilson, L., Sparks, R. S. J. and Walker, G. P.: Explosive volcanic eruptions—IV. The control of magma properties and conduit geometry on eruption column behaviour, Geophysical Journal International, 63(1), 117–148, doi:10.1111/j.1365-246X.1980.tb02613.x, 1980.~~

Yang, K., Liu, X., Bhartia, P. K., Krotkov, N. A., Carn, S. A., Hughes, E. J., Krueger, A. J., Spurr, R. J. D., Trahan, S. G.: Direct retrieval of sulfur dioxide amount and altitude from spaceborne hyperspectral UV measurements: Theory and application, J. Geophys. Res., 115, D00L09, doi:10.1029/2010JD013982, 2010.

Acknowledgements

The research leading to these results has received funding from the European Research Council under the European Union's Seventh Framework Programme (FP/2007–2013)/ERC Grant Agreement no. 279802. We wish to thank Daniele Morgavi and Jorge E. Romero for providing the Calbuco tephra samples and Jonathan Fellowes for helping with the petrological analyses. We also thank the two anonymous reviewers for the constructive comments to the original version of the manuscript.

Author contributions

F.P. and M.B. conceived this work, F.P. produced the numerical code with advice from G.L.S., performed all simulations and produced the manuscript with advice from all co-authors. F.A. contributed to the petrological elements of the paper.

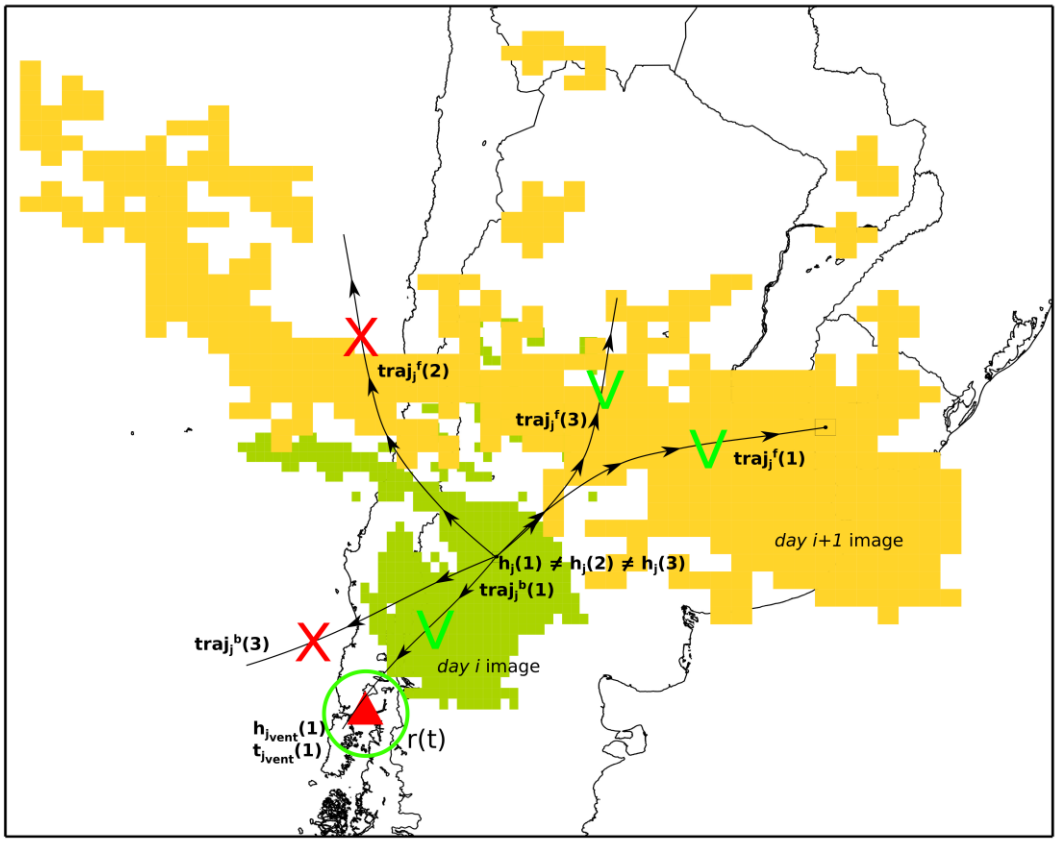
traj$_j^f$(2)
traj$_j^f$(3)
traj$_j^f$(1)
day *i+1* image
h$_j$(1) ≠ h$_j$(2) ≠ h$_j$(3)
traj$_j^b$(1)
traj$_j^b$(3)
day *i* image
h$_{jvent}$(1)
t$_{jvent}$(1)
r(t)

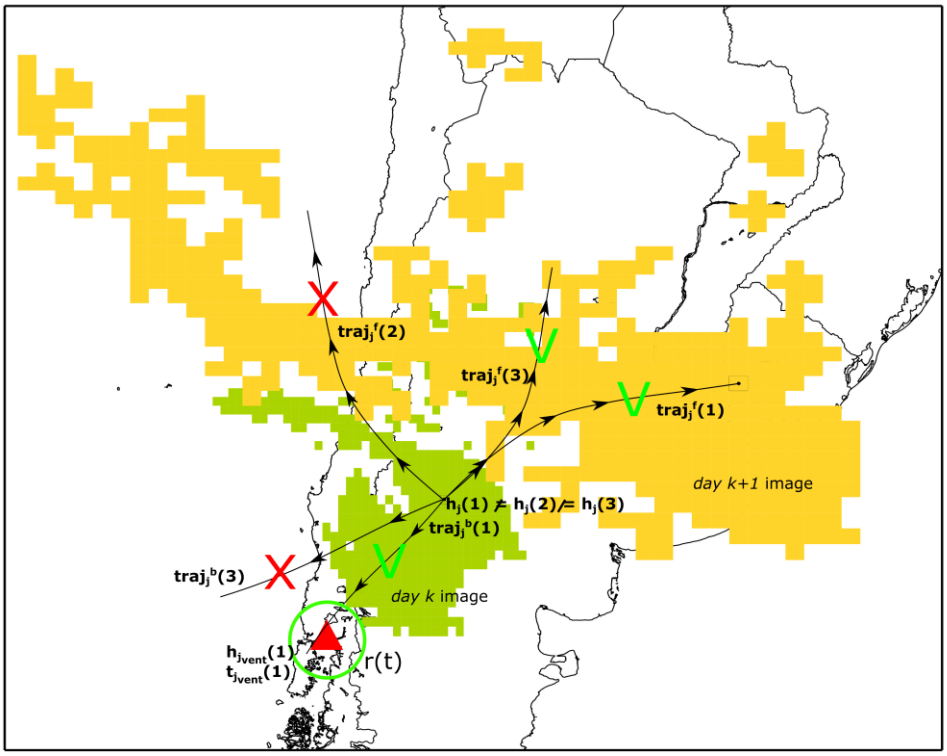

Figure 1. Schematic representation of the numerical procedure. Green pixels are those associated with the *day ~~i~~ k* satellite image, while yellow pixels are those from the *day ~~i~~k+1* image. From pixel *j*, trajectories traj$_j^f$(1), traj$_j^f$(2) and traj$_j^f$(3) are run forward from different staring altitudes (h$_j$(1), h$_j$(2) and h$_j$(3)). While traj$_j^f$(1) and traj$_j^f$(3) are consistent with the position of the plume at *day ~~i~~k+1*, traj$_j^f$(2) is not, thus it is neglected. Starting again from pixel *j*, traj$_j^b$(1) and traj$_j^b$(3) are initialized from altitudes h$_j$(1) and h$_j$(3) and are run backward in time. Only traj$_j^b$(1) is acceptable since it approaches the volcanic vent position at a distance less than *r(t)*.

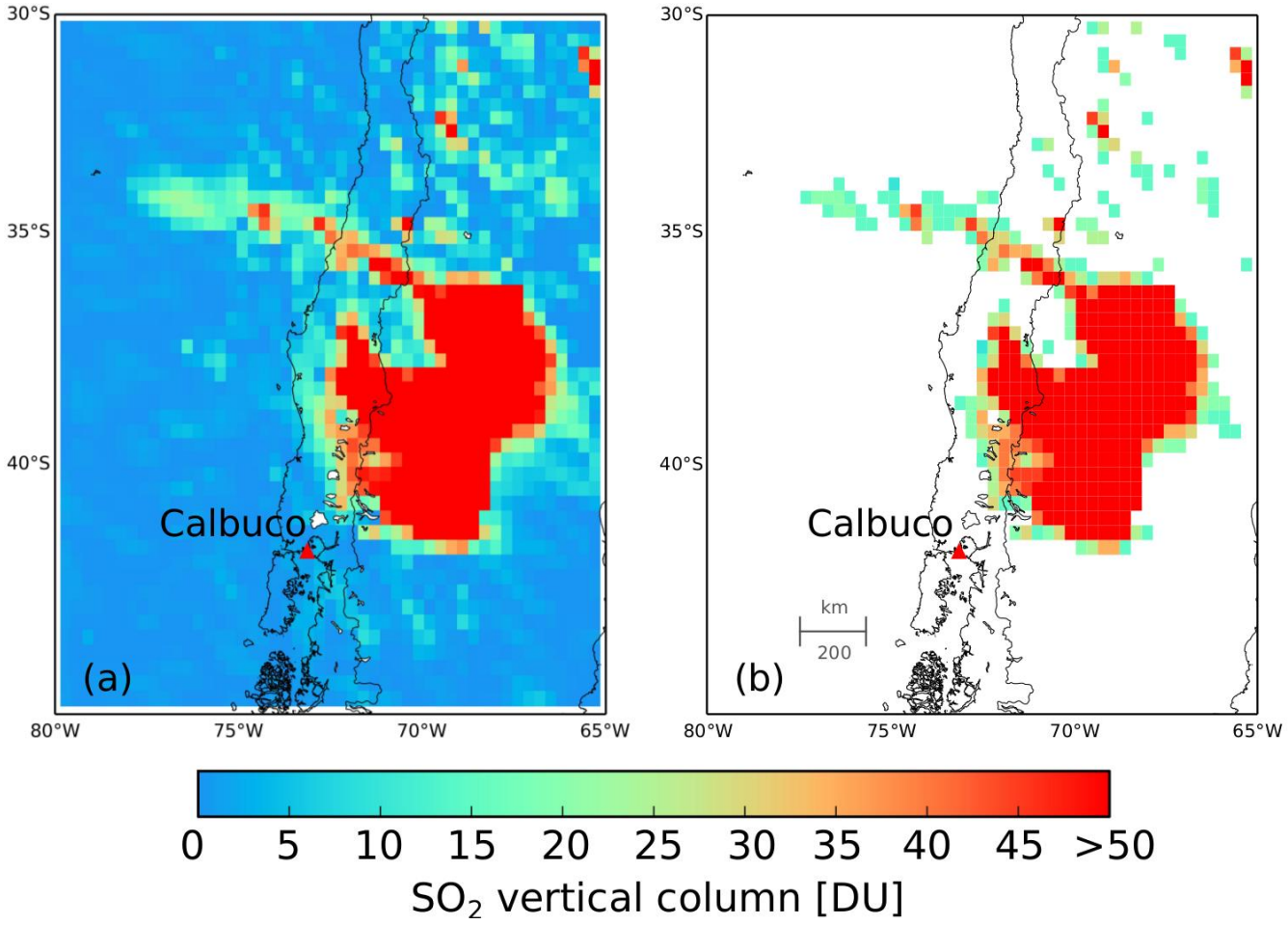

Figure 2. Calbuco SO_2 plume as seen by GOME-2 on 23 April 2015 ~~,~~assuming the plume is located at 2.5 km height, panel (a). ~~The 2.5 km is used as input for the numerical procedure.~~ Panel (b) presents the volcanic cloud extracted from the background noise.

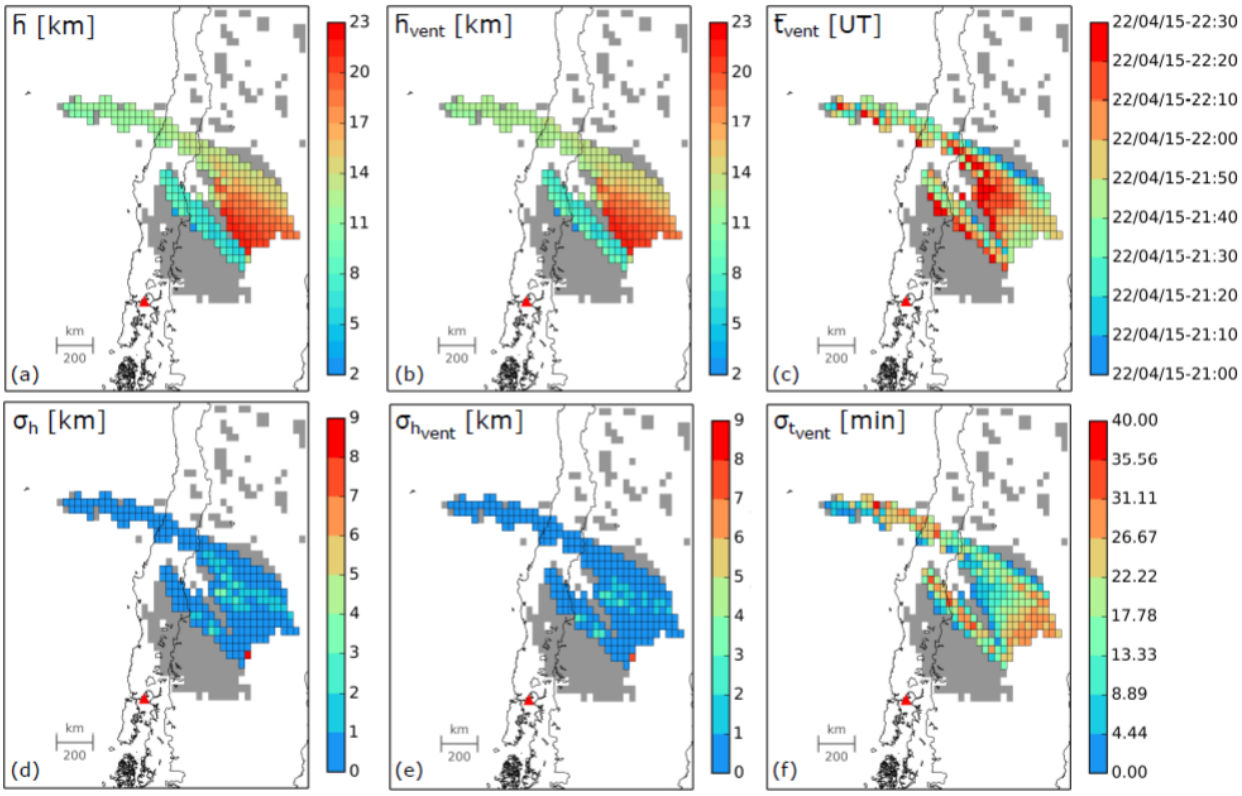
h̄ [km]
h̄vent [km]
t̄vent [UT]
σh [km]
σhvent [km]
σtvent [min]
(a)
(b)
(c)
(d)
(e)
(f)
km
200
23
20
17
14
11
8
5
2
9
7
6
4
3
1
0
40.00
35.56
31.11
26.67
22.22
17.78
13.33
8.89
4.44
0.00
22/04/15-22:30
22/04/15-22:20
22/04/15-22:10
22/04/15-22:00
22/04/15-21:50
22/04/15-21:40
22/04/15-21:30
22/04/15-21:20
22/04/15-21:10
22/04/15-21:00

5

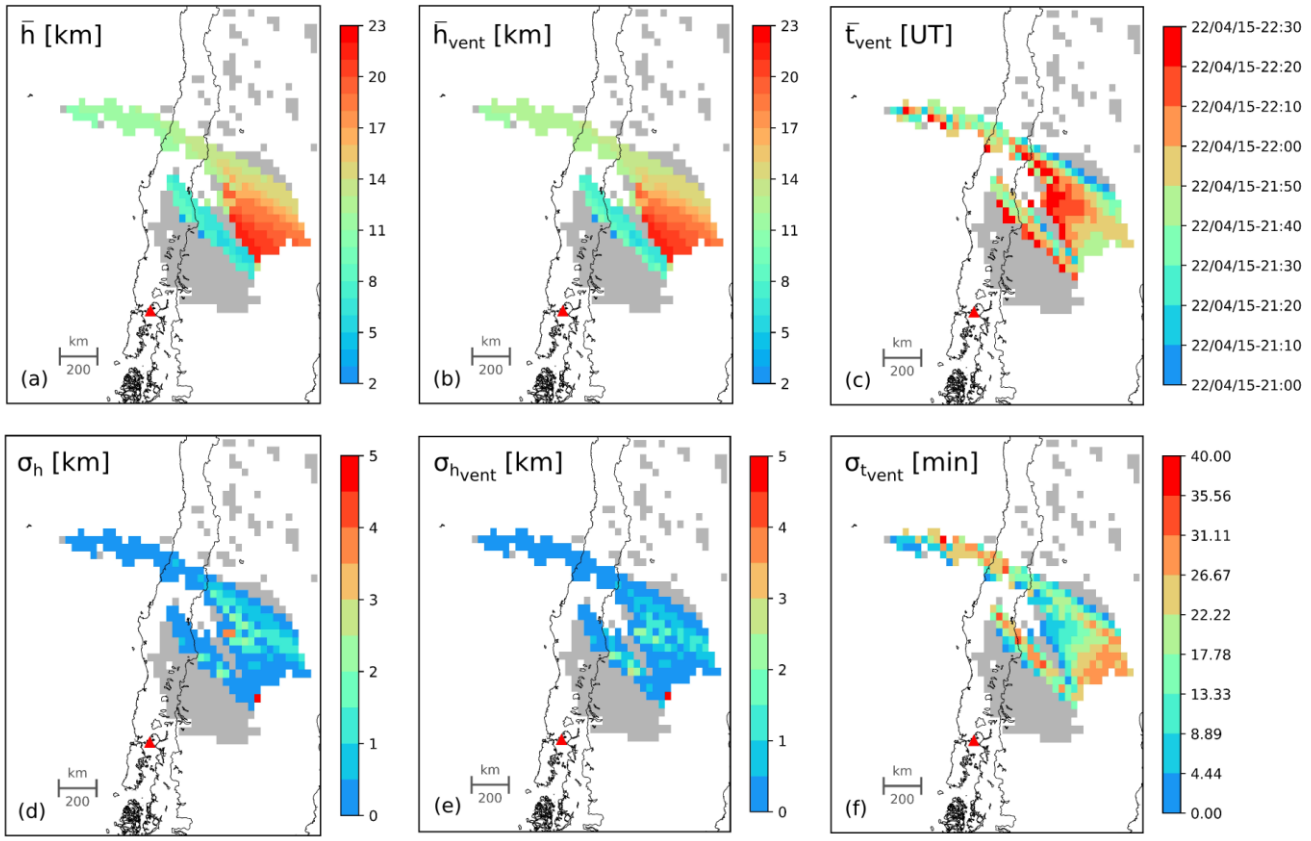

Figure 3. Calbuco SO_2 cloud emitted during Eruption 1 (considering trajectories approaching the vent from 21:00 to 22:30 on 22 April 2015). In panels (a), (b), and (c) mean plume height ($\bar{h}$), injection height ($\bar{h}_{vent}$) and injection time ($\bar{t}_{vent}$) are shown respectively. ~~For each pixel j, these values are computed as: $\bar{h} = \sum_{i=1}^{N} \frac{h_j(i)}{N}$, $\bar{h}_{j_{vent}} = \sum_{i=1}^{N} \frac{h_{j_{vent}}(i)}{N}$ and $\bar{t}_{j_{vent}} = \sum_{i=1}^{N} \frac{t_{j_{vent}}(i)}{N}$, where N is the number of trajectories that approach the vent, $h_j(i)$ is the altitude from which trajectories are initialized, while $t_{j_{vent}}(i)$ and $h_{j_{vent}}(i)$ are the time instant and the altitude of approach at vent position. In panels (d), (e) and (f) standard deviations are computed as: $\sigma_{j_h} = \sum_{i=1}^{N} \frac{(h_j(i)-\bar{h})^2}{N}$, $\sigma_{j_{h_{vent}}} = \sum_{i=1}^{N} \frac{(h_{j_{vent}}(i)-\bar{h}_{j_{vent}})^2}{N}$ and $\sigma_{j_{t_{vent}}} = \sum_{i=1}^{N} \frac{(t_{j_{vent}}(i)-\bar{t}_{j_{vent}})^2}{N}$.~~ A multi-layered plume emerges, with heights varying from 8 km to more than 20 km. Panels (d), (e) and (f) shown 1-sigma errors on retrieved plume heights, injection heights and injection time respectively. ~~Uncertainties on plume heights appear to be low, mainly between 0 and 1 km.~~

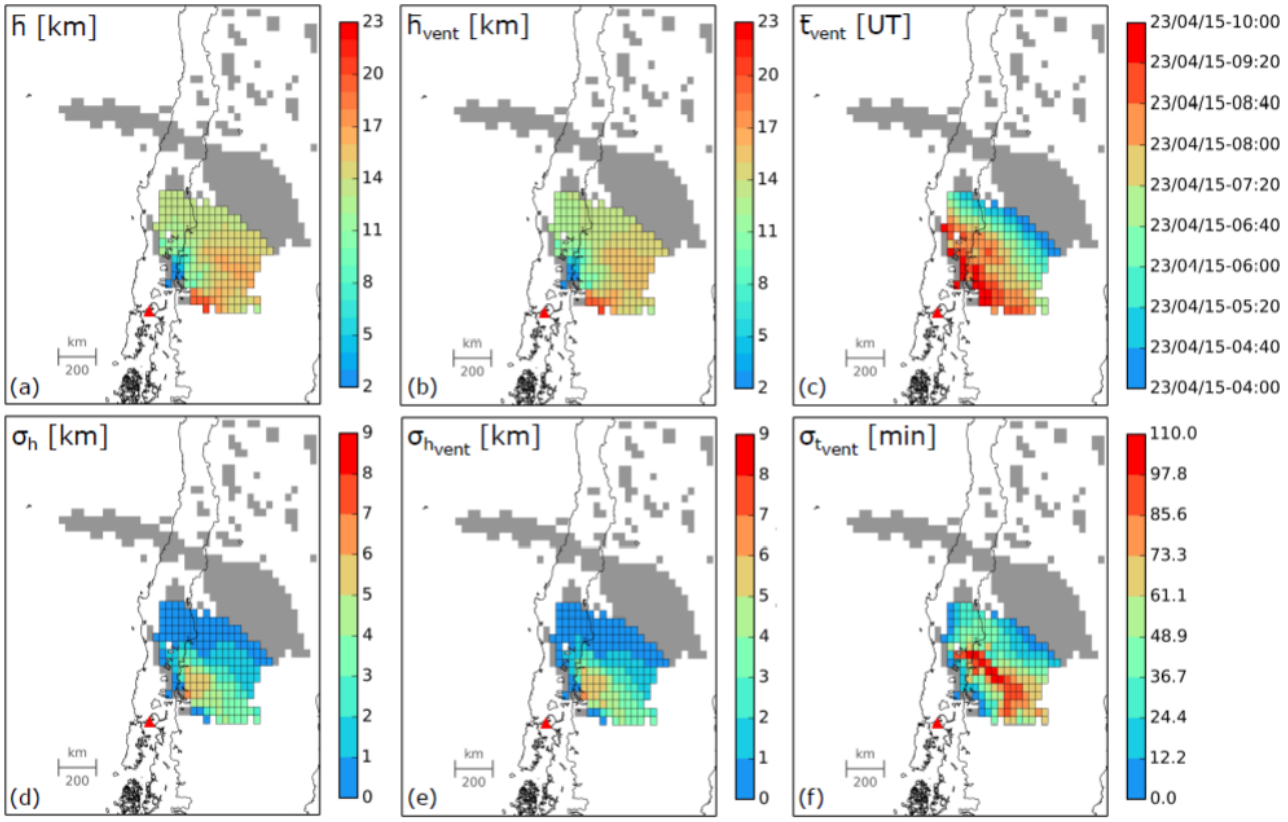
h̄ [km]
h̄vent [km]
t̄vent [UT]
σh [km]
σhvent [km]
σtvent [min]
(a)
(b)
(c)
(d)
(e)
(f)
km
200
23
20
17
14
11
8
5
2
9
8
7
6
5
4
3
2
1
0
110.0
97.8
85.6
73.3
61.1
48.9
36.7
24.4
12.2
0.0
23/04/15-10:00
23/04/15-09:20
23/04/15-08:40
23/04/15-08:00
23/04/15-07:20
23/04/15-06:40
23/04/15-06:00
23/04/15-05:20
23/04/15-04:40
23/04/15-04:00

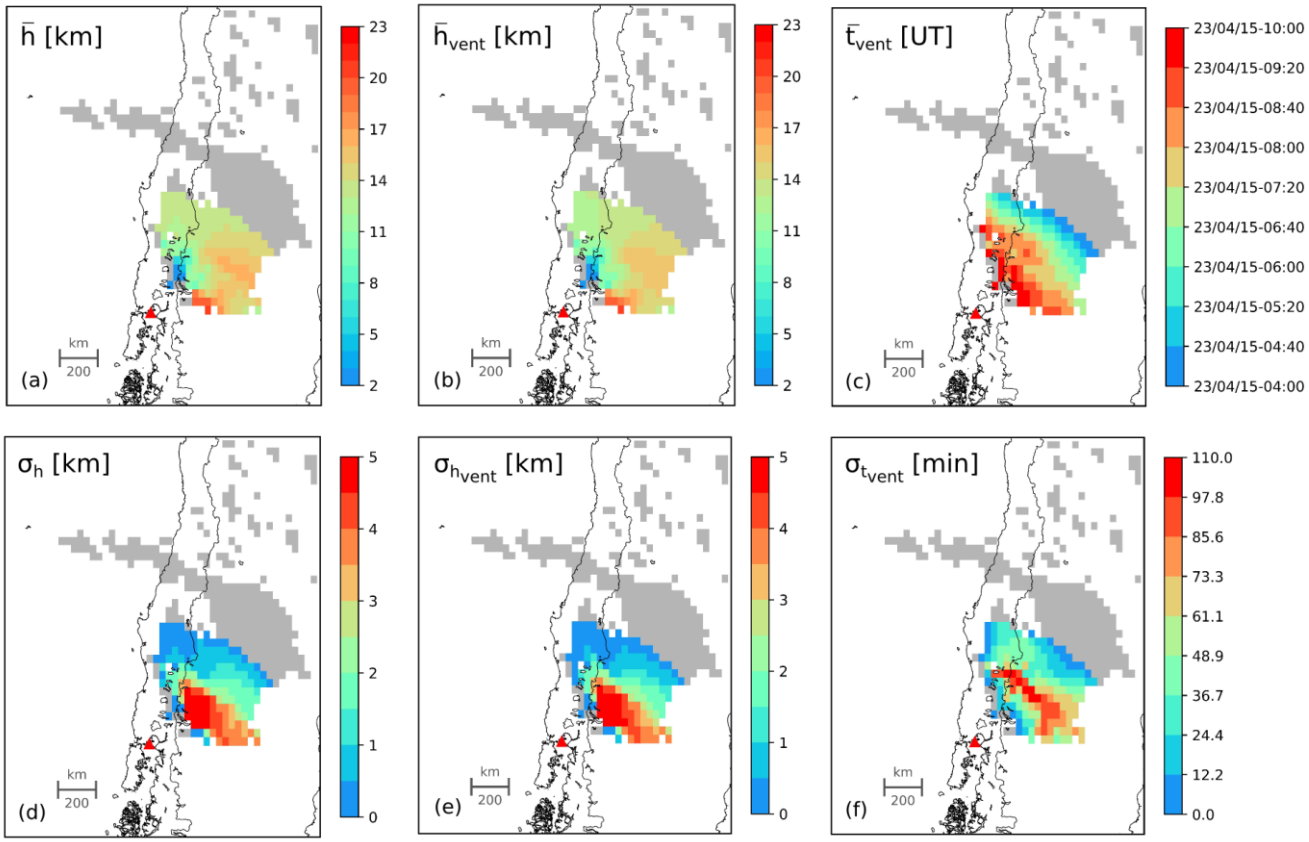

Figure 4. Calbuco SO_2 cloud emitted during Eruption 2 (considering trajectories approaching the vent from 04:00 to 10:00 on 23 April). ~~Plume heights and injection time are computed as shown for Eruption 1, see Figure 3.~~ Panels follow the same format as Figure 3. The SO_2 cloud appears to be located at ~14 km both at vent location and satellite overpass, ~~panels (a) and (b)~~ with a standard deviation of 2 km~~, panels (d) and (e)~~. The SO_2 injection time varies from 04:00 for pixels located ~~far~~furthest from the vent ~~position~~ to 10:00 for those closest~~r, panel (c)~~. Uncertainties on injection time are in the range 0-110 min with a mean value of 45 min~~, panel (f)~~.

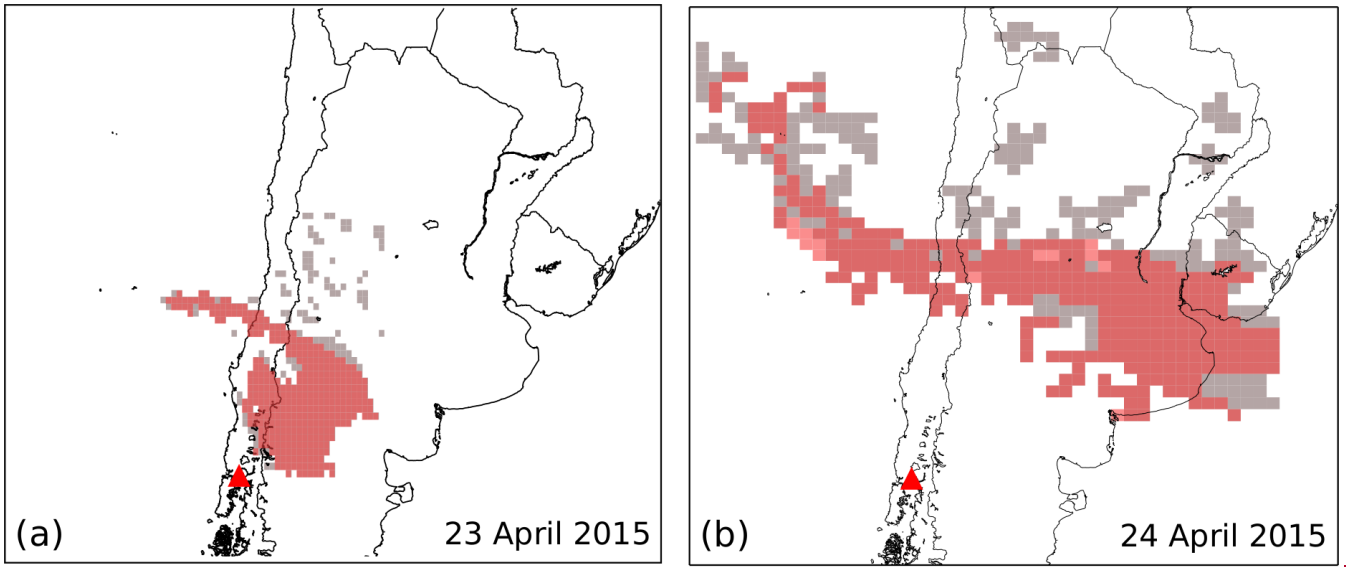

~~Figure 5.~~ ~~Red pixels in panel (a) are those for which at least one backward trajectory is accebtable and thus for which plume height, injection height and injection time can be computed. Grey pixels represent the computational domain. A good coverage for the solution is achieved excluding the sparse pixels located in the northern region of the domain. In panel (b) SO_2 cloud extracted from the 24 April image is shown (grey pixels). Red pixels are those consistent with the endpoints of the forward trajectory simulation performed in order to test the results.~~

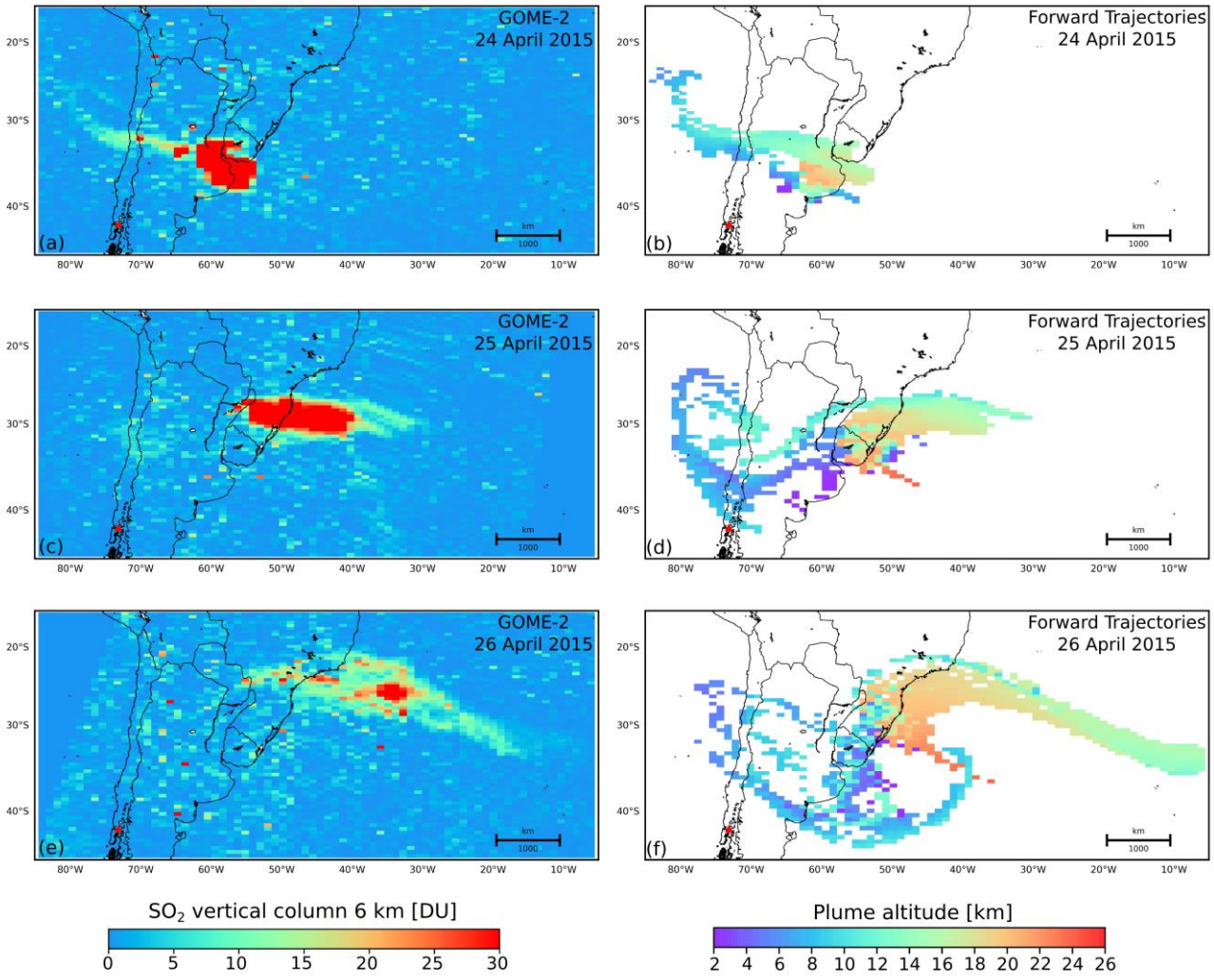

Figure 5. Comparison between the Calbuco SO_2 plume as seen by GOME-2 on 24, 25 and 26 April 2015, panels (a),(c),(e), and as retrieved from our numerical simulations, panels (b),(d) and (f).

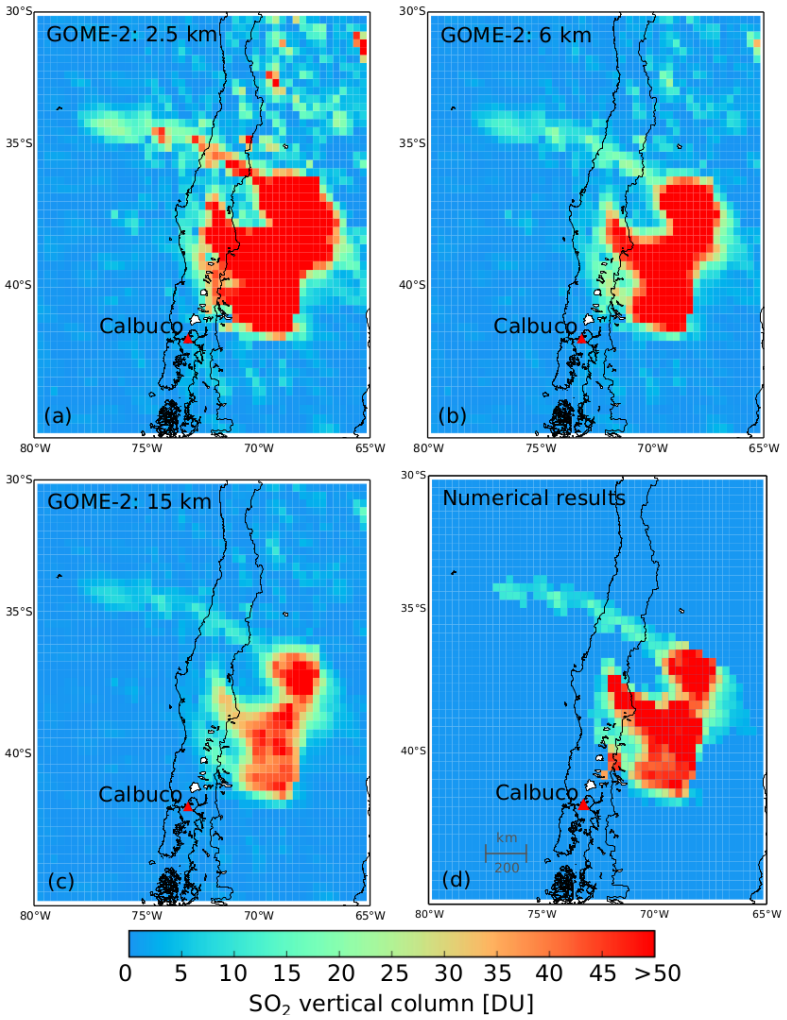

Figure 6. Vertical columns of Calbuco SO_2 plume as seen on 23 April 2015. Panels (a), (b) and (c) show retrievals performed by GOME-2 assuming plume heights of 2.5 km, 6 km and 15 km respectively. Panel (d) shows column amount corrected with ~~our numerical outcomes on~~ retrieved plume height. ~~A good match with the image in panel (c), 15 km retrieval, emerges.~~

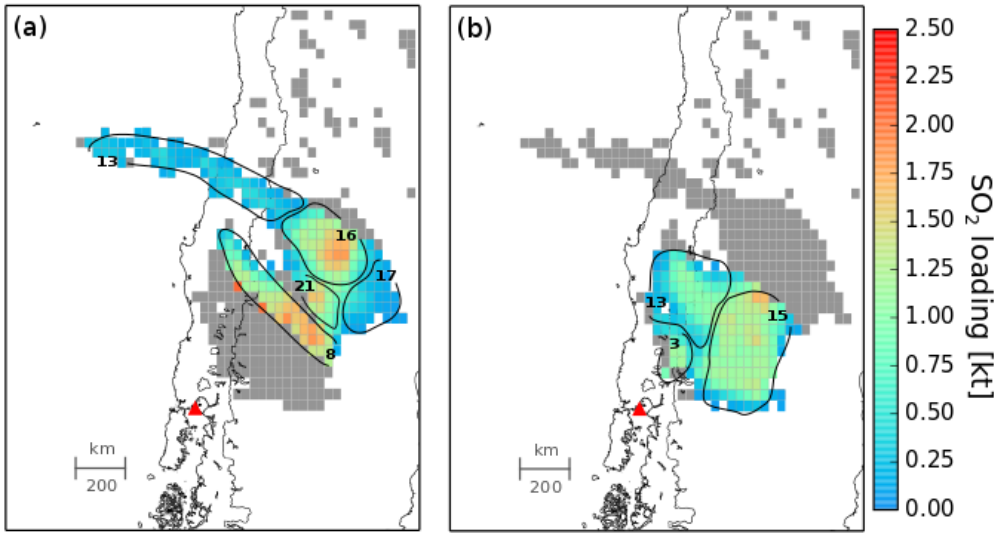

Figure 7. SO_2 loading computed for each pixel through linear interpolation at the retrived mean SO_2 height ($\bar{h}$). In panel (a) results for the cloud emitted during Eruption 1 are shown with the bulk of the SO_2 (83% of the total) injected into the atmosphere in the range 8-16 km, while the remain 17% between 17-21 km. Panel (b) presents results for the cloud emitted during Eruption 2. In this case 55% of the SO_2 is injected at 15 km, 41% at 13 km and the 4% at 3 km.

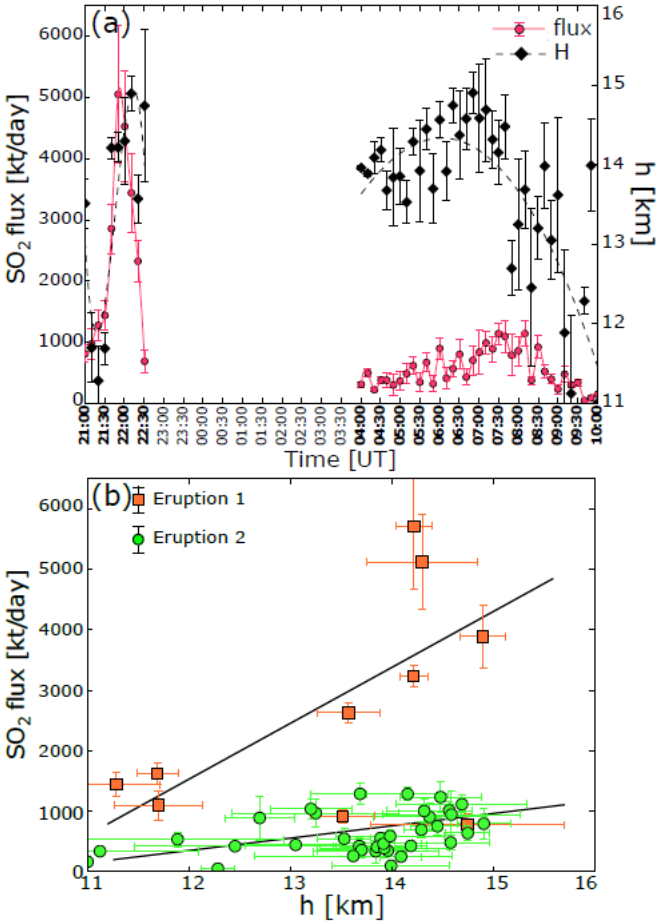

Figure 8. Panel (a) shows SO_2 flux time-series together with mean injection height time-series. SO_2 flux as a function of mean injection heights is shown in panel (b).

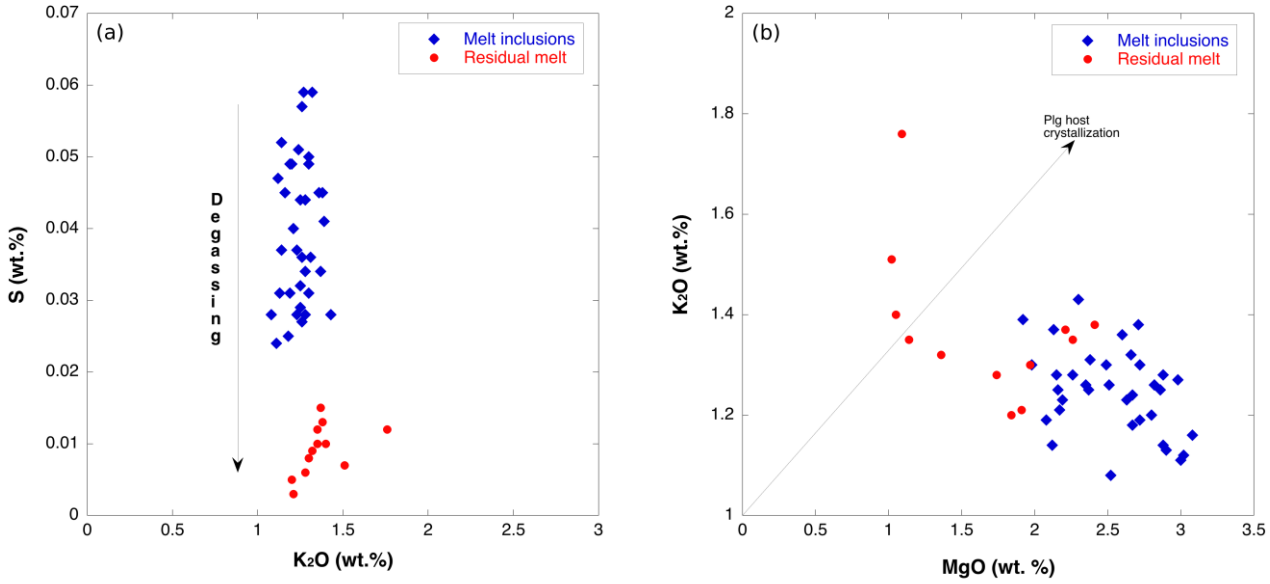

Figure 9: Variations of K_2O, MgO and S concentrations (in weight %) in melt inclusions (MIs) and residual melt in tephra samples of 2015 Calbuco eruptions. Panel (a) shows S vs. K_2O concentration in MIs and residual melt. The vertical arrow indicates S decrease caused by sulfur degassing. Panel (b) shows K_2O vs. MgO concentrations in MIs and residual melt. If plagioclase MIs are subject to host crystallization, both K_2O and MgO are enriched in MIs. Therefore, no post-entrapment crystallization occurred in MIs.

Table 1

	$m(SO_2)_{SAT}$	DRE	S_{MI}	S_{gm}	$m(SO_2)_{PETR}$ *	$m(SO_2)_{ex}$ **	$\%\ exsolved$
E 1	160±30 kt	0.036 km^3	0.035±0.01wt%	0.009±0.001wt%	38±12 kt	122±28 kt	76±20 %
E 2	140±35 kt	0.10 km^3	0.04±0.007wt%	0.01±0.003wt%	120±26 kt	20±38 kt	15±28 %

	$m(SO_2)_{SAT}$	M	S_{MI}	S_{gm}	$m(SO_2)_{PETR}$	$m(SO_2)_{ex}$	$\%\ ex$
E1	160±30 kt	6.2±2.2·10^4 kt	0.035±0.01wt%	0.009±0.0006 wt%	16±7 kt	144±26 kt	90±20 %
E2	140±35 kt	24±8.2·10^4 kt	0.04±0.007wt%	0.01±0.003 wt%	71±26 kt	69±39 kt	49±30 %

$m(SO_2)_{SAT}$, atmospheric sulfur yield as retrieved from satellite data.

M, mass of erupted solid material as estimated from our numerical method.

S_{MI}, S_{gm}, concentration of sulfur in melt inclusions and glassy matrix respectively.

*$m(SO_2)_{PETR} = \rho \cdot DRE\ M \cdot (S_{MI} - S_{gm}) \cdot \frac{MW(SO_2)}{MW(S)} \cdot 0.8(1 - CF)$, where ρ = 2450 kg m^{-3} M is the mass of erupted material, $MW(SO_2)$ and $MW(S)$ are the molecular weights of SO_2 and S equal to 64 g mol^{-1} and 32 g mol^{-1} and 0.8 CF is a coefficient accounting for 20 50 vol.% of phenocryst crystals (Arzilli et al., 2017)(Castruccio et al., 2016).

**$m(SO_2)_{ex} = m(SO_2)_{SAT} - m(SO_2)_{PETR}$, mass of pre-eruptive exsolved SO_2.

$\%\ ex = \frac{m(SO_2)_{ex}}{m(SO_2)_{SAT}} \cdot 100$, percentage of pre-eruptive exsolved SO_2.

Table 1: Calculation of SO_2 budget from Calbuco eruptions.